



## AN ABSTRACT OF THE THESIS OF

Marc Whitehead for the degree of Master of Science in Mechanical Engineering  
presented on June 18, 2013.

Title: Design and Manufacturing Study of Hydroelectric Turbines Using Recycled  
and Natural Fiber Composites

Abstract approved: \_\_\_\_\_

Roberto Albertani

The objective of this project is to demonstrate the feasibility fiber-reinforced turbine components through a design and manufacturing study. The motivation for using composites is to reduce weight and simplify manufacturing especially at high production volumes. In addition, natural fiber composites are implemented for applicable components to reduce environmental impact. Existing steel designs provided by major manufacturers are used as models. These are re-designed using composite materials, maintaining original geometry as much as possible. The components selected for composite design are the turbine penstock, scroll case, guide vanes, runner (impeller) and draft tube. In addition, the design of a composite fish ladder is presented to show the application of composites to other elements of hydroelectric power. Once the structural and mechanical design was complete, material and manufacturing costs were analyzed. The choice of materials was based upon loading requirements,

the runner required a high strength random reinforcement carbon fiber sheet molding compound (SMC) while a glass fabric and rovings provided adequate strength for the guide vanes, scroll case, penstock and outer walls of the fish ladder while minimizing the cost. A flax fabric was selected for the design of the draft tube additionally using a bio-based PLA resin. The inner sections of the fish ladder use a flax fabric and polypropylene pultrusion.

Manufacturing methods for each were selected based on geometry and cost. The complex shape of the runner was most easily formed using compression molding, which also reduced the cost as compared to hand lay up. A comparison between hand lay up and vacuum infusion was completed for the guide vanes and scroll case. Hand lay up was chosen for the draft tube as it is the most commercially proven method for the manufacture of components using natural fibers. Filament winding, the method used for the penstock would be the ideal method of manufacture but it has yet to be completed in a commercial setting with natural fibers.

Results show the cost of most parts is dominated by tooling (molds) for the components as the research focused on a small run of ten parts, assumed to be for research and testing purposes. However, the contribution of tooling can be cut in half if the run size is doubled. The design and manufacturing analysis does support the use of composite materials in hydroelectric turbines and the costs associated with their manufacture are within reasonable parameters for industry.

©Copyright by Marc Whitehead  
June 18, 2013  
All Rights Reserved

Design and Manufacturing Study of Hydroelectric Turbines Using  
Recycled and Natural Fiber Composites

by

Marc Whitehead

A THESIS

submitted to

Oregon State University

in partial fulfillment of  
the requirements for the  
degree of

Master of Science

Presented June 18, 2013  
Commencement June 2014

Master of Science thesis of Marc Whitehead presented on June 18, 2013.

APPROVED:

---

Major Professor, representing Mechanical Engineering

---

Head of the School of Mechanical, Industrial and Manufacturing Engineering

---

Dean of the Graduate School

I understand that my thesis will become part of the permanent collection of Oregon State University libraries. My signature below authorizes release of my thesis to any reader upon request.

---

Marc Whitehead, Author

## ACKNOWLEDGEMENTS

Thank you to my family for encouraging and inspiring me to pursue this degree and providing guidance in my life up to this point. Thank you also to my friends here in Corvallis for their excellent company and support, I have enjoyed all of our adventures; academic or otherwise. I would like to thank Dr. Albertani for welcoming me into his lab and, supporting and assisting me in my application for funding from the Hydro Research Foundation. He has continued to provide mentorship throughout my thesis, using his experience in the composite manufacturing industry to check my designs and process results. I would also like to thank Dr. Happala and Dr. Warnes for providing assistance on key elements of the project and sitting on my committee. Last but most definitely not least, I would like to sincerely thank the Hydro Research Foundation and the United States Department of Energy for providing the funding and industry connections that made this project possible. Specifically, thank you to Canyon Hydro for providing specifications for the two cases presented and Voith Hydro for providing turbine runner geometries. It has been a great experience and I have enjoyed the challenges and successes alike.

# TABLE OF CONTENTS

	<u>Page</u>
1 Introduction	
1.1 The Hydroelectric Industry . . . . .	1
1.2 The Need for New Development . . . . .	2
1.3 Project Goals . . . . .	3
2 Background and Literature Review	
2.1 Hydroelectric Turbines . . . . .	5
2.2 Composite Hydraulic Components . . . . .	14
2.3 Composite Design . . . . .	15
2.4 Composite Manufacturing . . . . .	20
2.5 Cost Estimation . . . . .	23
2.6 Natural Fibers . . . . .	24
2.7 Environmental Factors . . . . .	28
3 Materials and Methods	
3.1 Component Design and Manufacturing . . . . .	34
3.1.1 Penstock . . . . .	35
3.1.2 Scroll Case . . . . .	36
3.1.3 Guide Vanes . . . . .	38
3.1.4 Runner . . . . .	42
3.1.5 Draft Tube . . . . .	47
3.1.6 Fish Ladder . . . . .	49
4 Results and Discussion	
4.1 Manufacturing Process Results . . . . .	53
4.2 Cost Models . . . . .	55
5 Conclusion	
5.1 Feasibility results . . . . .	60
6 Future Work	62

## TABLE OF CONTENTS (Continued)

	<u>Page</u>
Bibliography	64
Appendices	72

## LIST OF FIGURES

Figure	Page
2.1 Bonneville dam Kaplan turbine component diagram. [4] . . . . .	6
2.2 The scroll case for radial flow machine. [20] . . . . .	7
2.3 The two Voith runners: a)Francis and b)Propeller geometries used for the FE and manufacturing analysis in this thesis. . . . .	11
2.4 The different runner profiles associated with a given specific speed [30].	12
2.5 The process of vacuum infusion on a vacuum bagged wind turbine blade[45] . . . . .	21
2.6 The process of impregnating fiber with resin during a wet lay up. [46]	21
2.7 The process of spray up manufacturing of composites. . . . .	22
2.8 The process of compression molding and a typical SMC used [49, 50].	31
2.9 The process of filament winding. [50] . . . . .	31
2.10 The process of pultrusion [54]. . . . .	32
2.11 Plot from Northrop study showing the time required to deposit woven fabric with respect to the area of a part. . . . .	32
2.12 Water jet created by a cavitation bubble imploding on a surface [76].	33
2.13 Common locations of cavitation erosion on a Francis runner. [77] . .	33
2.14 Common locations of cavitation erosion on a Kaplan runner blade. [77]	33
3.1 Model of the 2 MW Francis turbine. . . . .	35
3.2 Model of the 250 kW propeller turbine. . . . .	35
3.3 Drawing of the scroll case showing associated dimensions. . . . .	37
3.4 Isometric drawing of the scroll case to clarify shape. . . . .	37
3.5 The guide vane model with relevant dimensions tabulated on the right. $L$ and $b$ are the total length and height of the vane and $w$ is the width.	39

## LIST OF FIGURES (Continued)

<u>Figure</u>		<u>Page</u>
3.6	Comparison of a) CFD analysis of a Francis turbine blade and b) FEA analysis of a Francis blade from this project [34]. . . . .	44
3.7	Partitions made on the runner blade to prevent distorted meshing. . .	45
3.8	The mesh distribution allowed with the partitions. . . . .	46
3.9	Draft tube with associated dimensions. . . . .	48
3.10	Vertical slot fish ladder used as a model for the composite fish ladder in this project (non-SI units from literature). . . . .	50
3.11	Image highlighting the different parts of the fish ladder and their associated manufacturing techniques. . . . .	52
4.1	Cost of materials and labor for the 2MW turbine components. . . . .	56
4.2	Cost of materials and labor for the 250kW turbine components. . . . .	57
4.3	Costs of tooling for the 2MW turbine components. . . . .	57
4.4	Total cost for manufacture of components from both turbine cases. . .	59

## LIST OF TABLES

Table	Page
1.1 Hydropower feasibility and installed capacity around the world. [11] .	3
2.1 Range of dimensional specific speeds (in SI units) for specific turbine runner designs . . . . .	12
2.2 Mercedes-Benz automotive parts containing natural fibers [64]. . . . .	25
2.3 Vehicular use of natural fiber reinforced materials [64]. . . . .	25
2.4 Specific properties of e-glass and natural fibers. . . . .	28
3.1 Deflection, maximum Mises stress and relative safety factors for the Glass/Epoxy-Foam Core guide vane with comparisons for steel guide vanes. . . . .	41
3.2 Hashin damage criteria for tensile and compressive failure of the fiber and matrix for both guide vane models. . . . .	41
3.3 Design parameters for the comparison of the blade profile between the Voith runner geometry and Canyon case studies. . . . .	42
3.4 FE blade model results. . . . .	46
3.5 Dimensions for both draft tube cases. . . . .	48
3.6 Loads, chosen safety factor and calculated thickness for the composite draft tubes. . . . .	48
4.1 Summary of the manufacturing parameters for the 2 [MW] turbine case.	53
4.2 Summary of the manufacturing parameters for the 250 [kW] turbine case. . . . .	53
4.3 Weight differences between steel and composite components on a 2 MW Francis machine. . . . .	55
4.4 Weight differences between steel and composite components on a 250 kW propeller machine. . . . .	55

## LIST OF APPENDIX TABLES

<u>Table</u>	<u>Page</u>
1    Process model and person-hours for hand layup and vacuum infusion manufacturing methods for 2 <i>MW</i> wicket gate [55]. . . . .	73
2    Process model and person-hours for hand layup and vacuum infusion manufacturing methods for 250 <i>kW</i> wicket gate [55]. . . . .	74
3    Process model and person-hours for hand layup and vacuum infusion manufacturing methods for 2 <i>MW</i> scroll case [55]. . . . .	74
4    Process model and person-hours for hand layup and vacuum infusion manufacturing methods for 250 <i>kW</i> and 2 <i>MW</i> scroll case by HLU. . .	75
5    Tabulated costs for material, labor and tooling for the 2 <i>MW</i> turbine with totals for a 10 part run. . . . .	75
6    Tabulated costs for material, labor and tooling for the 250 <i>kW</i> turbine with totals for single unit in a 10 part run. . . . .	76

## Chapter 1: Introduction

### 1.1 The Hydroelectric Industry

Hydroelectric energy has been used to power grain mills for over 2000 years, long before James B. Francis invented the first Francis runner in 1840 [1, 2]. His work signaled the beginning of modern turbine design and since then the basic materials for constructing hydroelectric turbines have been stainless and standard carbon steel [3]. The properties of steel are well known and the methods of design and manufacture well practiced. Especially in large installations, from Bonneville at 1084 MW up to Hoover at 6,809 MW [4, 5], steel provides strength efficiently coupled with predictable fatigue and environmental damage resistance. However, in the current sustainability and preservation focused environment there is no drive to build large dams like those installed in the 50s. The desire to build small installations in locations that maximize the production of energy and the efficiency of transmission by reducing the distance between production and usage, while minimizing the impact on the environment, is growing. Distributed or Decentralized energy generation reduces the impact by reducing the need for transmission and reducing the energy production required to make up for transmission losses [6]. Small hydro also allows for a smaller initial capital investment and lower operation and maintenance costs, which allows for a quicker return on the initial investment [7, 8, 9]. Hydropower, as a generation method, has

the benefit of providing consistent energy, as compared to wind or solar that produce energy according to the cyclic availability of wind and sun. Also, the cost and size of hydropower devices relative to generating capacity is significantly better than other current renewable energy sources. It deserves note that while the physical size of the turbine is smaller the facilities still have an impact on the ecosystem. Research has shown that per unit of power generated, diversion based conventional small hydro has a larger impact than large reservoir hydro in the Nu valley in China [10]. This represents only one small hydroelectric facility design but it highlights the point that a smaller facility does not necessarily imply lower impact.

## 1.2 The Need for New Development

In the realm of sustainable energy, hydropower represents a consistent, reliable, low impact (when properly implemented) energy source that has the added benefit of facilitating irrigation in agricultural communities. The potential development for hydropower around the world is provided in table 1.1 below, which shows the potential *GWh*/year for all the continents of the world. Worldwide, only 10% of the economically feasible hydroelectric has been installed, which leaves a potential for development especially with new easily implementable designs.

Current turbine designs limit the feasibility of small, remote projects in their weight, cost and difficulty of maintenance and repair. Composite materials can greatly expand the ability of turbines to be installed in remote locations, where reliable transportation for heavy steel components is not available. In addition, the cost

Region (All numbers in [GWh/year])	Theoretically Feasible Hydropower	Technically Feasible Hydropower	Economically Feasible Hydropower	Installed Capacity	Technically Feasible to Installed	Economically Feasible To Installed
Africa	2,358,221	1,161,467	773,996	22,304	1.92%	2.88%
Asia	16,990,783	5,785,657	3,553,627	299,182	5.17%	8.42%
Australia	654,177	185,012	88,701	13,626	7.36%	15.36%
Europe	5,380,005	2,885,887	1,772,478	246,491	8.54%	13.91%
North & Cent. America	7,417,847	1,979,778	1,024,406	167,105	8.44%	16.31%
South America	5,778,880	26,060,408	1,558,523	138,644	0.53%	8.90%
World Total	38,606,913	14,604,209	8,771,502	887,352	6.08%	10.12%

Table 1.1: Hydropower feasibility and installed capacity around the world. [11]

of materials and manufacture for composites continue to decline as the methods of manufacture for components and raw materials become more streamlined. This, coupled with the relative ease of in-situ repair and damage tolerance, as demonstrated in CFRP bridge reinforcement and advanced composite repair in the aerospace and GFRP warship industries, makes them an economically attractive alternative from both an initial investment and O&M perspective [12, 13, 14].

### 1.3 Project Goals

This project aims to study the feasibility of designing turbine components using composite materials and demonstrates the benefits of using these materials in terms of weight savings, ease of installation and maintenance. Re-design of existing components with composite materials focuses on two cases; a 2 MW radial flow Francis machine and a 250 kW axial flow propeller machine. For each of these models the components designed from composites are the penstock, scroll case (for the Francis machine), stay vanes, runner and draft tube. Not including the generator, these components comprise the largest weight contribution to the power generating system and

are the main components of the hydraulic pathway. For each of these components, a steel reference component is designed and the loading analyzed to provide a baseline for the composite design. In addition, the design of a composite fish passage structure is presented in comparison with a current concrete design to demonstrate further applications of composites to hydroelectric facilities. Changes are made as needed to accommodate the use of composite materials, ensuring strength and maintaining the original geometry as much as possible. In parallel with the composite design, manufacturing processes are chosen that will allow each of the components to be manufactured as economically as possible. A cost analysis is then performed for each component to show the complete cycle of constructing components from composite materials. Where appropriate, natural fibers are implemented into the designs to decrease energy usage and pollutant production [15].

## Chapter 2: Background and Literature Review

### 2.1 Hydroelectric Turbines

The design of conventional hydroelectric turbines is well studied and reported in the literature, starting with the basic fluid mechanics of turbo machinery [16]. This review will provide an overview of pertinent design information regarding hydroelectric turbines following the flow path of water through the turbine. For reference, a turbine unit at Bonneville Dam near Portland, Oregon is displayed in figure 2.1. Water enters the turbine through the penstock, a pipe which connects the water reservoir to the turbine casing. The design of this pipe is based on the static pressure head between the tail race below the draft tube of the turbine and the fore bay (water level in the reservoir) determined by Bernoulli's equation

$$p = \rho gh \quad (2.1)$$

where  $\rho$  is the density of the fluid in kilograms per meter cubed,  $g$  is the acceleration of gravity in meters per second squared and  $h$  is the net head in meters. This equation assumes head losses are small for a low flow, low head system. The hoop stress on the penstock can then be calculated using

$$\sigma_{\theta} = \frac{pr}{t} \quad (2.2)$$



Figure 2.1: Bonneville dam Kaplan turbine component diagram. [4]

where the hoop stress  $\sigma_\theta$  in pascals is given by the pressure  $p$  in pascals multiplied by the outer radius  $r$  divided by the thickness  $t$  in meters [17]. The thickness can be varied to ensure that the component is within allowable stress determined by the material properties and given factor of safety.

After the water enters the scroll case (a more detailed image of the scroll case is provided in figure 2.2) it enters two sets of guide vanes that re-direct the flow onto the turbine impeller known as a runner [18]. These blades direct the flow so that the maximum amount of kinetic energy is transferred to the runner. The scroll case is shaped in order to maintain a constant velocity, and therefore load on the runner, around the entire circumference of the case. As with the penstock, the design of the



Figure 2.2: The scroll case for radial flow machine. [20]

case is based on the static pressure head from the reservoir with a factor of safety to account for a water hammer - a sharp increase in pressure due to a rapid shutoff of the turbine required if there is an equivalent drop in electrical load on the machine causing the runner to exceed its design speed [19]. The first set of guide vanes in the turbine are fixed, welded or bolted to the top and bottom surfaces of the spiral case. The second set, known as the wicket gates, can be rotated to alter the flow direction based on operating conditions to maximize turbine efficiency. These gates can cause a water hammer if they are shut too quickly to avoid adverse operating conditions. The design of stationary gates is based on the hydrodynamic pressure load created by flow through the turbine [21]. The shape of these vanes is the same as an airfoil so the loading can be calculated using Von Mises equations for airfoils [22].

$$L = \frac{\rho}{2} V_o^2 S C_L \qquad D = \frac{\rho}{2} V_o^2 S C_D \qquad (2.3)$$

The lift  $L$  and drag  $D$  in Newtons are given by the velocity of the fluid multiplied by its density  $\rho$ , The plan-form area  $S$  is the reference area,  $S = Bc$ , (the length of the span of the gate multiplied by its chord length) and the coefficients of lift and drag,  $C_l$  and  $C_d$  which can be taken from empirical data on airfoils.  $V_o$  is the velocity of the fluid flowing around the gate, in meters per second, parallel to the chord direction (assuming the angle of attack is measured from the chord of the hydrofoil). The radial component of the velocity,  $V_{or}$  can be calculated using the flow rate through the turbine divided by the area of the flow passage at the diameter of the wicket gates and then  $V_o$  can be determined trigonometry assuming the angle of fluid flow is close the angle of attack of the wicket gate. This gives velocities

$$V_{or} = \frac{Q}{\pi(gcd)} \qquad V_o = \frac{V_{or}}{\sin(\alpha)} \qquad (2.4)$$

in a radial turbine and

$$V_{or} = \frac{Q}{\pi(r_1^2 - r_2^2)} \qquad V_o = \frac{V_{or}}{\sin(\alpha)} \qquad (2.5)$$

for an axial turbine [19] where  $Q$  is the flow in  $m^3/s$ ,  $gcd$  is the gate circle diameter in m and  $r_1$  and  $r_2$  are the interior and exterior diameters of the axial turbine flow channel in meters. The loads were applied to the respective gates modeled as an asymmetrical loaded beam and the resultant load from the lift and drag forces was calculated and applied to the beam as an asymmetric distributed load, following the method in [23]. The angle  $\phi$  of the plane of loading with respect to the  $x$ -axis is calculated by knowing that the lift and drag are perpendicular and parallel

respectively to the velocity vector, which makes an angle of attack  $\alpha$  to the profile of the hydrofoil. This gives  $\phi$  as

$$\phi = -\left(\frac{\pi}{2} + \alpha\right) + \tan^{-1}(D/L) \quad (2.6)$$

Knowing the angle of the plane of load with respect to the reference coordinate system allows us to calculate the angle of the neutral axis  $\alpha_2$  of the cross section using the moments of inertia

$$\alpha_2 = \frac{I_x}{I_y} \cot \phi \quad (2.7)$$

The moment on the beam, assumed to be fixed at both ends, is calculated using the formulas in [24]

$$M = \frac{b^2 w}{12} \quad (2.8)$$

We need the x-component of this moment to calculate the maximum normal stress on the surface of the beam. Since  $M$  is oriented at  $\phi$  with respect to the coordinate system, this gives

$$M_x = M \sin \phi \quad (2.9)$$

With these values and the moments of inertia for the cross section, we can calculate

the maximum tensile and compressive stresses using

$$\sigma_a = \frac{M_x(y_A - x_A(\tan \alpha))}{I_x - I_{xy}} \tan \alpha \quad \sigma_b = \frac{M_x(y_B - x_B(\tan \alpha))}{I_x - I_{xy}} \tan \alpha \quad (2.10)$$

where  $A$  and  $B$  are the points on the outer edge of the gate profile furthest from the neutral axis in the positive and negative directions. The tensile stress is higher as its distance is further from the neutral axis.

After the water passes through the gates it reaches the turbine runner. While the operating principles are the same, the turbine runner comes in different forms based on the operating conditions of the turbine. The best runner designs for low head applications are the Francis and Propeller. The latter is familiar to most as it is in the shape of a typical propeller used on boat, the former was designed by James B. Francis in 1840 and has become the most common runner design in the world today [2]. Images of these two runner designs are presented in figure 2.3 [25]. The design of the runner blades is based on inlet and exit angles accompanied by computational fluid dynamics (CFD) modeling. The load on the blade is due to the pressure load from the water and the inertial load from the rotation of the runner. If the power of the machine is known, then the load can be calculated using the formula below

$$L = \frac{P}{rNn_b} \quad (2.11)$$

where the Load  $L$  in newtons is given by the power of the machine  $P$  in watts divided by the distance of center of the runner from the hub multiplied by the speed of the

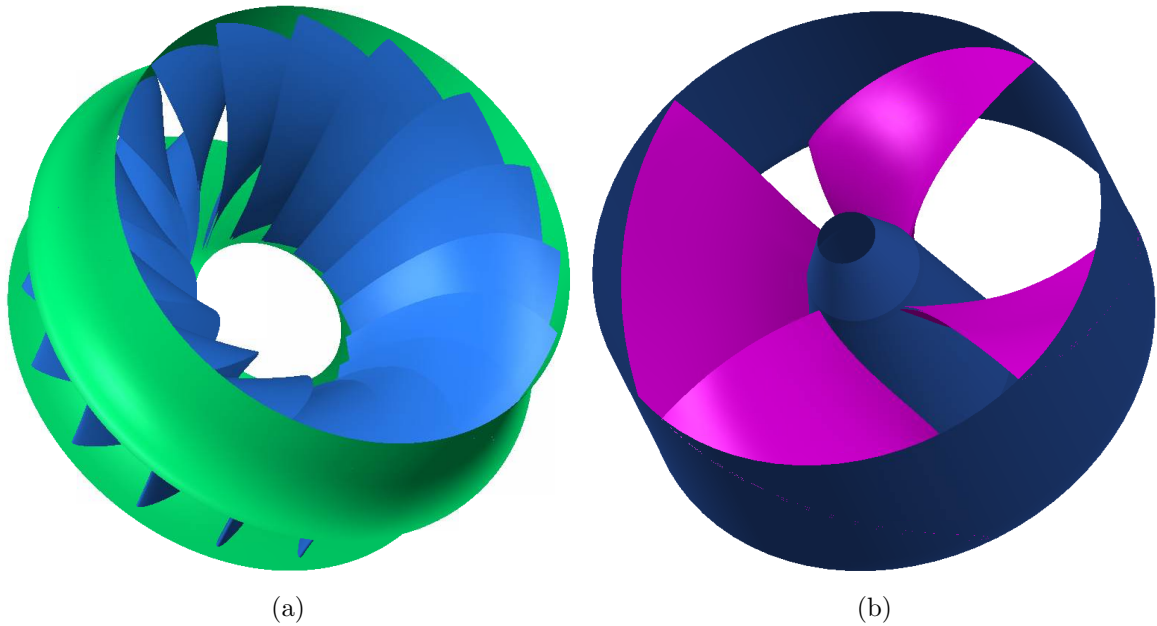


Figure 2.3: The two Voith runners: a)Francis and b)Propeller geometries used for the FE and manufacturing analysis in this thesis.

unit  $N$  in rps (revolutions per second) and the number of blades  $n_b$ . This assumes 100% efficiency and most runners are in the neighborhood of 95% efficient water to wire (net head of the turbine to electrical energy leaving the generator) [26, 27, 28].

Given models of varying size, dimensionless parameters are used to assist in scaling models and determining the basic profile of the runner blades [29]. Specifically, the aspect ratio of the runner blades is determined by the specific speed of the runners, given by

$$P = \rho QgH \qquad N_s = \frac{N\sqrt{P}}{H^{5/4}} \qquad (2.12)$$

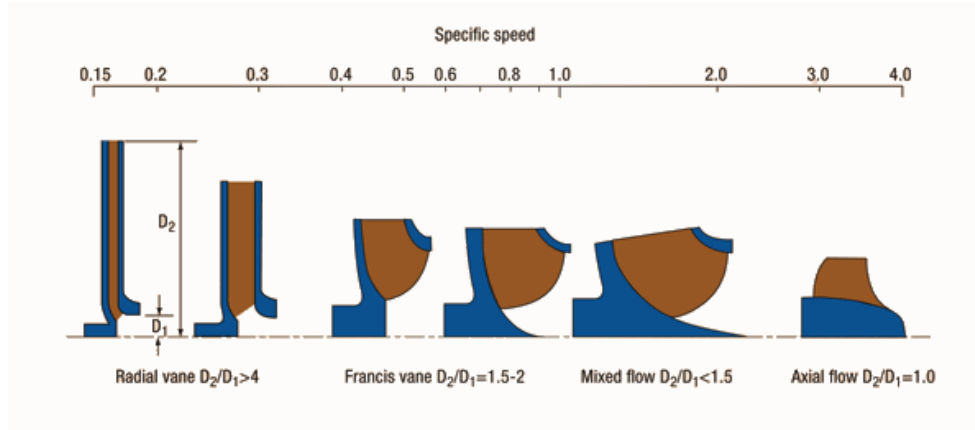


Figure 2.4: The different runner profiles associated with a given specific speed [30].

which is the dimensional specific speed commonly used in industry, which requires careful attention to ensure units are kept consistent. The specific speed is the power  $P$  multiplied by the rotational speed of the turbine  $N$  in revolutions per second (*rps*) divided by the pressure head of the turbine  $H$  in m. The power is calculated knowing the flow  $Q$  and the head of the turbine as noted above. The specific speeds associated with different runner types are presented in table 2.1 and the different blade profiles associated with given specific speeds are shown in figure 2.4. The values in figure 2.4 are for the dimensionless specific speed, which can be converted to dimensional by

Runner Type	$N_s$ (SI Units)
Single Jet Pelton	8-29
Twin Jet Pelton	26-40
Multiple Jet Pelton	40-67
Radial Flow Francis	67-450
Axial Flow Kaplan	364-970

Table 2.1: Range of dimensional specific speeds (in SI units) for specific turbine runner designs

multiplying the values at the bottom of the figure by  $\rho^{1/2}g^{1.2} = 549$ .

When the water exits the turbine, it passes through a diffuser known as the draft tube. Assuming total efficiency the water will have minimal pressure when it leaves the turbine. The draft tube creates a head of suction between the discharge ring of the casing and the tailwater below the turbine; this suction further increases the efficiency of the turbine by pulling water through the turbine and into the tailrace. The design of the draft tube is based on this vacuum load, which is given by Bernoulli's equation

$$\frac{p_2}{\rho g} = \frac{p_{atm}}{\rho g} - \left( H_s + \frac{v_2^2}{2g} - \frac{v_4^2}{2g} - h_{suc} \right) \quad (2.13)$$

where  $H_s$  is the suction head between the discharge ring and tailrace and  $h_{suc}$  is the head loss given by

$$h_{suc} = k' \frac{v_2^2}{2g} \quad (2.14)$$

with the loss coefficient  $k'$  taken from design tables in and the velocities are calculated using  $V = Q/A$  at both of the sections (2 being at the discharge ring of the casing and 4 being at the bottom of the draft tube).

Given the vacuum, it is also important to calculate the critical pressure for buckling of the draft tube. This is done by modeling the draft tube as a simple cylindrical pressure vessel of constant profile at the maximum diameter and applying the maxi-

mum vacuum load. The critical pressure is given by

$$P_{cr} = \frac{E}{12 * (1 - \nu^2)} \left(\frac{t}{r}\right)^3 \left[ n^2 - 1 \frac{2 * n^2 - 1 - \nu}{-1 + n^2 l^2 / \pi^2 r^2} \right] + \frac{Et}{r} \left[ \frac{1}{(n^2 - 1)(1 + n^2 l^2 / \pi^2 r^2)^2} \right] \quad (2.15)$$

where  $E$  is the modulus of the material used,  $\nu$  is the Poisson's ratio,  $n$  is the buckling mode, the lowest 2 is selected as higher orders will not occur in a structure that is only fixed at the ends, and  $t$ ,  $r$  and  $l$  are the radius, thickness and length of the draft tube in m [31].

## 2.2 Composite Hydraulic Components

The literature surrounding the design of composite turbines focuses primarily on tidal and wave turbines as they benefit from the low density, high specific properties, economy of scale and corrosion resistance of composites given their large size and the corrosive environment of the ocean. They also have higher loading requirements than conventional turbines, supporting the design of composite conventional hydroelectric turbines [32]. The designs presented were for a 1.5 MW commercial scale turbine using a sandwich construction with a glass fiber reinforced polymer (GFRP) skin and a carbon fiber reinforced polymer (CFRP) spar cap necessitated by the significant bending loads produced by the water flow over the blade.

Another design used a form of filament winding (FW), a process for manufacturing

composites that wraps fiber dipped in a resin bath around a mandrel, to construct a composite marine current turbine [33]. This project also completed a combined CFD and FE analysis of the turbine runner, proving the feasibility of the model. CFD analysis has also been performed on conventional turbine blades made from steel to assist in further blade profile design refinement to increase efficiency and reduce damage due to cavitation [34]. This work showed how basic design parameters could be used to create a preliminary blade design, which could then be imported into a CFD program that would apply the correct loading on the blade and through an iterative loop, refine the geometry to maximize efficiency.

Composites are commonly used in industrial settings when the environment is highly corrosive. The fiber reinforced plastic (FRP) pipe industry has well defined parameters for designing fiberglass piping [35, 36]. These standards describe the calculation of thicknesses similarly to steel piping except they include a much higher factor of safety (10) as compared to the steel industry (2 or less). Despite the increased the thickness, the overall cost for installation of fiberglass piping can be less than equivalent steel, especially in exposed scenarios where the steel pipe would already require bracing and supports [13].

### 2.3 Composite Design

Fiber-reinforced composites combine a matrix, which provides structure, with fibers to provide the needed strength and stiffness. The combination produces parts with high specific properties at low densities, which far exceed the capabilities of either of the

constituent parts [37]. The common fibers are glass, carbon and aramid (Kevlar<sup>®</sup>), which are typically combined with a polymer matrix. These matrices can be thermoset, such as polyester, vinyl ester and epoxy, which cure and cannot be remelted or thermoplastic such as polypropylene, which can be remelted and reformed multiple times with little reduction in properties [38]. Composite parts are often made using uni-directional layers of fibers, known as plies when they are cured, oriented at different angles to achieve the required stiffness and strength in different directions. This creates an anisotropic material, which requires a more involved design and analysis. A quasi-isotropic lay up is commonly used in situations in which the loading is highly variable. This layup creates a laminate, whose properties do not vary with respect to direction in-plane. Common quasi-isotropic layups are shown in equation 2.16.

$$[0^\circ/90^\circ/ + 45^\circ/90^\circ/ - 45^\circ]_s \qquad [0^\circ/ + 60^\circ/ - 60^\circ]_s \qquad (2.16)$$

where the orientation of lamina within a laminate are noted with respect to a reference direction, commonly the major axis of the component, and the  $s$  implies that the 0, 90, and two 45 degree plies are all repeated symmetrically with the  $s$  being the middle of the laminate. For example, the second of equation 2.16 would have six plies at  $0^\circ$ ,  $+60^\circ$ ,  $-60^\circ$ ,  $-60^\circ$ ,  $+60^\circ$  and  $0^\circ$  degrees.

While the laminate may appear isotropic in-plane, the component lamina are still anisotropic and failure can occur at specific plies due to specific load scenarios that

stress one ply more than another. Many theories have been developed to describe the failure in fiber-reinforced composites. Beginning with a theory developed by Hankinson for the uniaxial compressive strength of spruce [39]. Many other theories have followed but the most common theories applied today are those developed by Tsai-Hill and Hashin [40, 41, 42]. The former is quite accurate but requires the determination of normal-shear stress interaction parameters that require a complex set of material parameters to be determined before the criteria can be applied. Hashin's failure criteria does not include these interaction parameters and can overestimate strength especially in combined shear and normal compression [43, 44]. However, it only requires the compressive and tensile strength the in longitudinal and transverse directions, as well as the shear strengths in these directions and so it has risen to prominence in research and industry.

The Hashin criteria differentiates failure by fiber rupture and failure of the matrix, in both tension and compression. The criteria for plane stress, assumed for most thin-skinned composites, are

$$\begin{aligned}
 F_f^t &= \left( \frac{\sigma_{11}}{\sigma_A^+} \right)^2 + \left( \frac{\sigma_{12}}{\tau_A} \right)^2 = 1 \\
 F_f^c &= \frac{\sigma_{11}}{\sigma_A^-} = 1 \\
 F_m^t &= \left( \frac{\sigma_{22}}{\sigma_T^+} \right)^2 + \left( \frac{\sigma_{12}}{\tau_A} \right)^2 = 1 \\
 F_m^c &= \left( \frac{\sigma_{22}}{\tau_T} \right)^2 + \left[ \left( \frac{\sigma_T^-}{2\tau_T} \right)^2 - 1 \right] \frac{\sigma_{22}}{\sigma_T^-} + \left( \frac{\sigma_{12}}{\tau_A} \right)^2 = 1
 \end{aligned} \tag{2.17}$$

The associated variables are defined as:

$F_f^t$  = failure in fiber mode in tension

$F_f^c$  = failure in the fiber mode in compression

$F_m^t$  = failure in the matrix mode in tension

$F_m^c$  = failure in the matrix mode in compression

$\sigma_A^+$  = tensile failure stress in the fiber direction

$\sigma_A^-$  = compressive failure stress in the fiber direction

$\sigma_T^+$  = tensile failure stress in the transverse direction

$\sigma_T^-$  = compressive failure stress in the transverse direction

$\tau_T$  = transverse failure shear

$\tau_A$  = axial failure shear

The criteria are satisfied (failure initiated) when the value is 1 or greater. The criteria were chosen to be quadratic to allow them to be fit to data, which is primarily quadratic in form. The theory is based on that fact that all fiber-reinforced composites are transversely isotropic. Given an orthogonal coordinate system with fibers in the  $x_1$  direction, material properties will be invariant under rotations in the  $x_2$  and  $x_3$  directions. This means that for a given loading scenario, stress invariants can be

defined as follows

$$\begin{aligned}
I_1 &= \sigma_{11} \\
I_2 &= \sigma_{22} + \sigma_{33} \\
I_3 &= \sigma_{33}^2 - \sigma_{22}\sigma_{33} \\
I_4 &= \sigma_{12}^2 + \sigma_{13}^2 \\
I_5 &= 2\sigma_{12}\sigma_{23}\sigma_{13} - \sigma_{22}\sigma_{13}^2 - \sigma_{33}\sigma_{12}^2
\end{aligned} \tag{2.18}$$

Omitting  $I_5$  because it is cubic, the most general quadratic function that can be written from these invariants is

$$A_1 I_1 + B_1 I_1^2 + A_2 I_2 + B_2 I_2^2 + C_{12} I_1 I_2 + A_3 I_3 + A_4 I_4 = 1 \tag{2.19}$$

This function estimates failure for all loading situations in every direction in the most general case but for fiber-reinforced composites we can differentiate between loading that will cause fiber failure and that which will cause matrix failure. Hashin's criteria simplifies equation 2.19, respectively, for the fiber and matrix as

$$A_f \sigma_{11} + B_f \sigma_{11}^2 + \frac{1}{\tau_A^2} (\sigma_{12}^2 + \sigma_{13}^2) = 1 \tag{2.20}$$

$$A_m (\sigma_{22} + \sigma_{33}) + B_m (\sigma_{22} + \sigma_{33})^2 + \frac{1}{\tau_T^2} (\sigma_{23}^2 + \sigma_{22}\sigma_{33}) + \frac{1}{\tau_A^2} (\sigma_{12} + \sigma_{13}^2) = 1 \tag{2.21}$$

recognizing that only  $\sigma_{11}$ ,  $\sigma_{12}$  and  $\sigma_{13}$  loads will cause fiber failure, while  $\sigma_{22}$ ,  $\sigma_{13}$  and  $\sigma_{23}$  will only affect the matrix. These two equations are further broken down into tensile (2.22) and compressive (2.23) failure for the fiber and matrix failure modes, with approximations made to accommodate only having one equation (the second of

2.22) to determine the two coefficients, as

$$\left(\frac{\sigma_{11}}{\sigma_A^+}\right)^2 + \frac{1}{\tau_A^2}(\sigma_{12}^2 + \sigma_{13}^2) = 1 \quad (2.22)$$

$$\sigma_{11} = -\sigma_A^-$$

$$\frac{1}{\sigma_T^{+2}}(\sigma_{22} + \sigma_{33})^2 + \frac{1}{\tau_T^2}(\sigma_{23}^2 - \sigma_{22}\sigma_{33}) + \frac{1}{\tau_A^2}(\sigma_{12}^2 + \sigma_{13}^2) = 1$$

$$\frac{1}{\sigma_T^-} \left[ \left(\frac{\sigma_T^-}{2\tau_T}\right)^2 - 1 \right] (\sigma_{22} + \sigma_{33}) + \frac{1}{4\tau_T^2}(\sigma_{22} + \sigma_{33})^2 + \frac{1}{\tau_T^2}(\sigma_{23}^2 - \sigma_{22}\sigma_{33}) + \frac{1}{\tau_A^2}(\sigma_{12}^2 + \sigma_{13}^2) = 1 \quad (2.23)$$

Finally, if we assume plane stress then all terms including the  $x_3$  direction are dropped and we achieve the criteria listed in equations 2.17.

## 2.4 Composite Manufacturing

Composite manufacturing is based on combining the fiber and resin in the most efficient proportion to produce a strong, stiff part. The method that requires the lowest equipment investment and understanding is hand lay up (HLU). Dry fabric is laid down in a mold in the shape of the part and resin is poured over and pressed in with rollers to wet the fabric, which is then cured at room temperature or in an oven/autoclave [38]. Another method which uses dry fiber is vacuum infusion (VI), the dry fiber is laid into the mold, held in place by stitches and/or a tacky spray. The complete lay up is covered with a bag and a vacuum is drawn using fittings cut through the bag. Resin injection fittings are also added and once the vacuum is

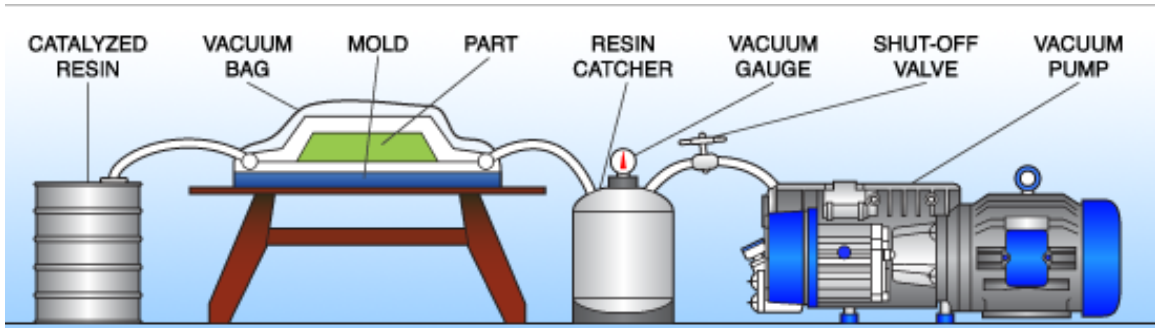


Figure 2.5: The process of vacuum infusion on a vacuum bagged wind turbine blade[45]

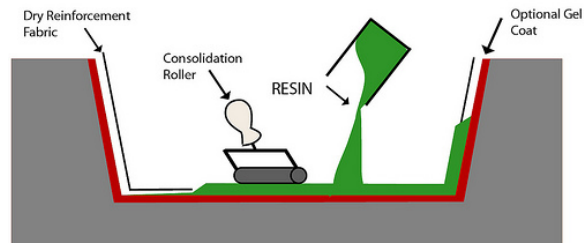


Figure 2.6: The process of impregnating fiber with resin during a wet lay up. [46]

confirmed to be sealed, resin is supplied through the lines to impregnate the fabric. VI significantly reduces the labor costs as compared to hand lay up. Images of the processes for HLU and VI are illustrated in figures 2.6 and 2.5.

Spray up manufacturing is a less labor intensive manufacturing method that allows for quick deposition of large amounts of material for applications with lower strength requirements. The process uses a gun, which propels chopped fiber through a spray of resin and then onto the part as shown in figure 2.7. The deposited material is compacted with rollers and then left to cure similar to a hand layup.

A further level of automation is achieved by compression molding, which uses a hydraulic press to conform a resin and fabric combination, sheet molding compound

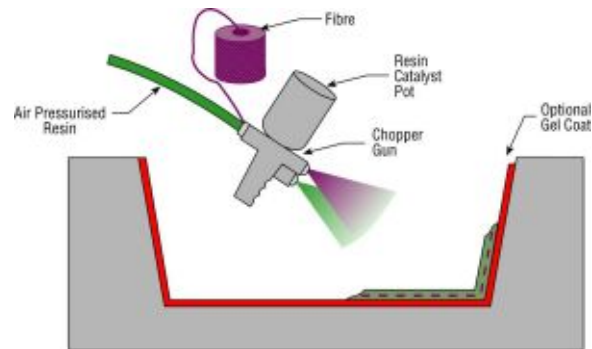


Figure 2.7: The process of spray up manufacturing of composites.

(SMC) is common, to the shape of matched die molds as shown in figure 2.8 a) and an image of a randomly reinforced chopped carbon prepreg SMC is also shown in b) of the same figure [47, 48].

The molding of thick components using prepreg SMC is referred to as a Forged Composite<sup>®</sup> [51]. The process is the same as compression molding of SMC but requires larger presses to ensure that the necessary pressure is applied to the part to ensure consistent distribution of fiber and resin.

Two more pertinent processes are pultrusion and filament winding. Filament winding, mentioned earlier, pulls rovings (groups of parallel aligned fibers) through a resin bath and guides them onto a rotating mandrel. This process is the best choice for convex, rotationally symmetric parts such as the nose cones of airplanes and pressure vessels [38, 52]. An image showing the process of filament winding is presented in figure 2.9. Pultrusion pulls a similarly wetted fiber through a heated die, typically 90 to 100 cm long, which cures the part. This process creates parts of constant profile and is one of the most efficient methods of manufacturing composite parts [53]. The process for pultrusion is illustrated in figure 2.10, which also shows

how parts can be cut to specific lengths using an automated cut off saw.

## 2.5 Cost Estimation

The most detailed process model for composites was completed by the Northrop Corporation, which collected data on the time required to perform each step in the manufacturing process and used the power law to fit curves to the data and create equations that would allow for future estimation based on a given variable. For example, the curve comparing the time required to lay a piece of woven fabric with its area is presented in figure 2.11. The curve is associated with an equation  $T_l = 0.000751A^{.6295}$ . Some processes use linear functions and others include a fixed set-up time but the principle is the same throughout the work [55]. The Northrop study has remained an industry standard despite its age [56].

A case study comparison of VI and prepreg lay up was completed by Gurit [57]. This study has process models for both methods of manufacture and show the time required for infusion. It also cites the cost for labor in both of these processes at \$39/hr. The time required for VI has also been studied on smaller scale parts including fiber glass boat hulls, which required 45 mins. to infuse for a 7.62 m yacht [58]. Other cost estimation uses basic rules of thumb to determine labor time, specifically HLU and chopped fiber spray up, which are estimated at 4 *kg/hr* and 20 *kg/hr* respectively [47, 59]. The labor and material costs of filament winding are examined in a study comparing prepreg filament winding to wet filament winding of pressure vessels, this work shows that wet filament winding costs \$11.63/kg [52]. The cost of materials

can be acquired from commercial sources and compared with reviews of composite manufacturing completed in academia [48, 60].

The cost of molding, commonly known as tooling, is also presented in case studies on manufacturing from academia [48]. This work provides multiple industry guided studies that show the cost of all steps in the development of a mold for a number of different parts including a die for pultrusion, jet engine cowling and helicopter rotor blades. For compression molding, the cost of tooling, labor and materials is compiled in a computer model [61, 62]. This model uses inputs of projected and total area, thickness and weight to calculate the cycle time, labor, and cost of tooling for compression molding. A comparison for this work is provided by cost estimation used in the plastics industry [63]. This model uses a point system to determine the complexity and thickness of the mold, which in turn define the amount of machining required to produce these high volume molds, which can produce well over 50,000 parts.

## 2.6 Natural Fibers

Natural fibers (NF) have been extensively researched as reinforcements for composites but their commercial use has been limited to semi-structural applications, most notable in the automotive industry [64]. Tables 2.2 and 2.3 show the different locations of NF and the amount used in different models from Mercedes-Benz. In 2000, it also began using NF for the exterior engine panels of its Travego and TopClass engine compartment structures.

<b>Interior Parts</b>	<b>Natural Fibers Used</b>
Glove Box	Wood/cotton fibers molded, flax/sisal (W203RH)
Door Panels	Flax/sisal/wood fibers with epoxy resin/UP matrix
Instrument panel support	Wood fiber molded material
Seat coverings	Leather/wool backing
Seat surface/backrest	Rubber hair (coconut fiber/natural fiber)
Seat backrest panel	Cotton fiber
Trunk panel	Cotton with PP/PET fibers
Trunk floor Kombi	Laminated wood
Insulation	Cotton fiber
Molding rod/apertures	Wood
<b>Exterior Parts</b>	
Floor panels	PP-NMT (flax) W168:released, no series

Table 2.2: Mercedes-Benz automotive parts containing natural fibers [64].

<b>Interior Parts</b>	Model year	No. of parts	Weight [kg]
Mercedes-Benz			
C Class	2000	33	22.0
S Class	1998	32	24.6
E Class	1995	21	20.5
A Class	1997	27	11.9
C Class	1992	30	18.3
Other Manufacturers			
BMW Series 3	1998	-	12.0
Audi A4(B6)	1999	-	10.0
VW Passat	1997	-	2.0
Audi A4(B5)	1993	-	1.5
<b>Exterior Parts</b>			
Mercedes-Benz			
Travego	2000	3	12.3
TopClass	2000	3	14.1

Table 2.3: Vehicular use of natural fiber reinforced materials [64].

More recently Daimler-Chrysler has been investing in research and development of flax-polyester composites for exterior applications. A truck with flax-based skirting panels is now in production. Tests carried out by Daimler's research group in Germany have shown that natural fiber based composites have excellent impact resistance, not shattering into splinters like their synthetic glass counterparts. This was the same property that Henry Ford enjoyed when promoting his soybean based trunk lids by striking them with an axe [65]. Daimler-Chrysler also noted good dimensional stability and weather resistance in its natural fiber based composites. The largest results of Daimler's research were an exterior wheel cover for its A-class vehicle in 2005 and the transmission/engine cover for the Travego coach. The latter created a 10% savings in weight and a cost reduction of 5% over synthetic fibers. The natural fibers used in the Travego were about a third the cost of the glass roving at the time they were purchased in 2002 [64].

The most significant utilization of natural fibers in the automotive industry so far is Lotus' Eco Elise released in 2008. The vehicle uses Hemp, Eco wool and Sisal throughout the interior and exterior. One of the main advances is the Eco Elise's use of Hemp to create the class 'A' structural composite body panels. The class 'A' finish is the surface finish level with the lowest defects and the highest water resistance, Lotus is one of the first manufacturers to achieve this level of quality with natural fibers. The Eco Elise serves as an excellent proof of concept for the use of natural fibers in high quality structural exterior applications [66]. Literature relating to the manufacture and mechanical properties of flax and other natural fiber composites is presented below.

Pultrusion and compression molding of natural fiber composites was completed with a flax/polypropylene yarn [67]. This work showed that the resulting pultrusion had strengths between 60-120 MPa and moduli of 4-10 GPa. The work noted that the flax fibers required significant drying to ensure good adhesion with the hydrophobic resin. Pultrusions using natural fibers have also been completed on an industrial scale with similar properties [68]. Filament winding of natural fibers is not common in industry but has been studied in academia [69]. It was shown that natural fibers alone have very high stiffness, comparable to glass fibers, but processing needs to be refined. Results showed that filament wound disc tensile strength was only 25-29% of comparable glass fiber composites. Other work has reviewed natural fiber composites on a broader scale, discussing properties of many different layup combinations [70, 71]. The results of this work showed strength and stiffness for hand lay up of Flax/PLA were on the lower boundary of the numbers presented by [67]. Another study also compared properties for a variety of fibers with a polyester matrix [72]. This study showed that Jute had the highest strength at  $43.0 \pm 6$  MPa for a hand lay up using a random fiber mat with other fibers being 30 MPa and below with some hardly increasing the strength of the neat matrix. A final interesting study showed that in an overall evaluation of the process of manufacturing natural fiber composites less energy was expended and pollutants produced as compared to the manufacture of glass composites [15]. This study notes that the lower strength of natural fiber composites requires a higher fiber content which lowers the percentage of the composite that must be made of the energy intensive and pollution creating polymer. However, this higher fiber content still retains a lower overall weight as

certain natural fibers have higher specific properties than glass fibers as shown in table 2.4. The main problem in designing strong composites from natural fibers is engineering the fiber/resin interface. Natural fibers are by nature very hydrophilic while most synthetic resins are hydrophobic. To create strong bonds between the natural fibers and the resins, it is necessary to chemically or mechanically treat the fibers to create bond sites [73, 74].

	E-glass	Flax	Hemp	Ramie
$\rho[kg/m^3]$	2.55E3	1.400E3	1.480E3	1.500E3
$\sigma_{max}[MPa]$	2400	800-1500	550-900	500
$\sigma_{max}[\frac{GPa \cdot m^3}{kg}]$	941	821	490	333
$E[GPa]$	73	60-80	70	44
$E/\rho[\frac{GPa \cdot m^3}{kg}]$	29	26-46	47	29

Table 2.4: Specific properties of e-glass and natural fibers.

## 2.7 Environmental Factors

Cavitation causes significant damage to the runner blades and, in certain cases turbine inlet and guide vanes [75]. Cavitation is created when the pressure of the water in a reaction turbine drops below the vapor pressure for a given temperature. The drop in pressure creates small bubbles of water vapor, which will be reabsorbed when the pressure rises. Cavitation causes no adverse effects when it occurs in free stream flow but when it occurs at the surface of material, the vapor bubble can implode against the surface creating a water jet, as shown in figure 2.12 that can increase the pressure at that point up to 500 MPa. Cavitation occurs in specific areas on the turbine due

to different geometric and operating parameters. The three main types of cavitation in reaction turbines are:

- Inlet edge cavitation
- Interblade vortex cavitation
- Traveling bubble cavitation

Common locations of cavitation in Francis and Kaplan turbines are shown in 2.13 and 2.14 [77].

The mathematical analysis presented in the literature shows that cavitation can generally be avoided by keeping the turbine within its designed operating range. However, given that the turbine will likely be run outside design parameters at times, research has also been completed on cavitation resistant coatings for metals and composites [78, 79]. Work completed using the ASTM G32 vibratory induced cavitation test has shown that two elastomer based coatings, Biocoat-A and PLV 2100 #4 were the most cavitation resistant with erosion rates of  $2.80 \mu\text{m}/\text{hr}$  and  $3.05 \mu\text{m}/\text{hr}$  respectively compared with 316 stainless steel which erodes at a rate of  $2.28 \mu\text{m}/\text{hr}$ . Uncoated composites can have cavitation rates two or three orders of magnitude larger than coated specimens. The Army Corps of Engineers performed a study on the use of coatings as opposed to conventional repair by welding, which cost \$676,239.17 at Green Peter Dam outside of Detroit, OR over the course of 10 years of maintenance. The coatings require less equipment to be lowered into the spiral casing and can be completed more quickly.

Hygroscopy, the absorption of water by a material, is another concern for synthetic fiber-reinforced composites. The matrix is the primary pathway of water absorption [80]. Recent research investigated the use of epoxy-carbon composites in aircraft. It was found that after a composite laminate absorbs water there will always be some retention regardless of the effort to bake out moisture [81]. It was hypothesized that this is due to the plasticizing behavior of water in polymer matrices. They also noted that there was less water absorption in submerged samples compared to those subjected to a 95% RH environment and that the rate of water absorption and total absorption decreased (the latter nearly 30%) for the temperatures in hydroelectric turbines ( $< 35^{\circ}\text{C}$ ). Composites have significant and successful usage in the aerospace industry and this research shows that for the conditions in hydroelectric turbines the hygroscopic nature of the matrix would have less of an effect on the performance of the laminate.

An even more relevant example of hygroscopy in composites is their use in the marine environment. Fiberglass is a common material for the construction of boat hulls and has been used successfully since the advent of fiberglass composites in the 1940s as noted by [82]. There is literature describing methods of protection from hygroscopy using water resistant gel coats for boat hulls [83].

Pultruded jute/polyester composites have absorption rates of up to 15% of their total and weight. The absorption and the swelling that results can reduce the strength of the composite up to 30% reduction in strength compared with dry samples [84]. Also, the product life of natural fiber based composites is not well known

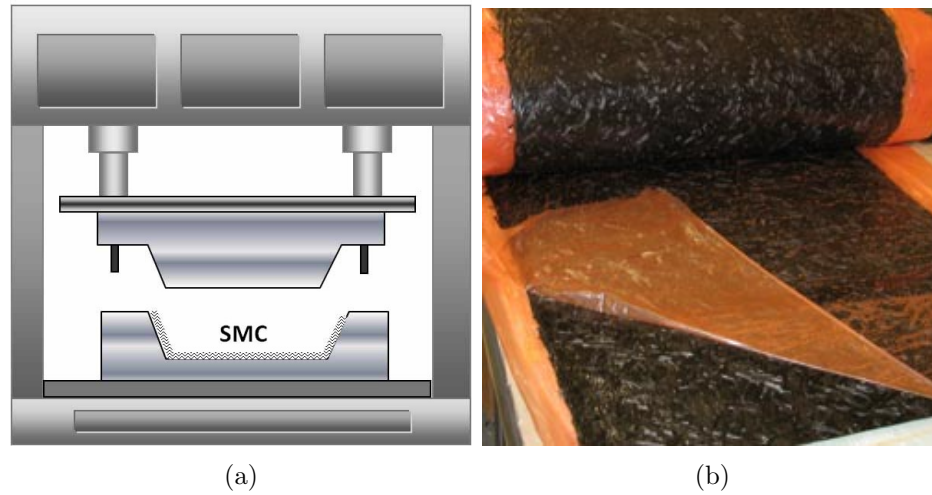


Figure 2.8: The process of compression molding and a typical SMC used [49, 50].

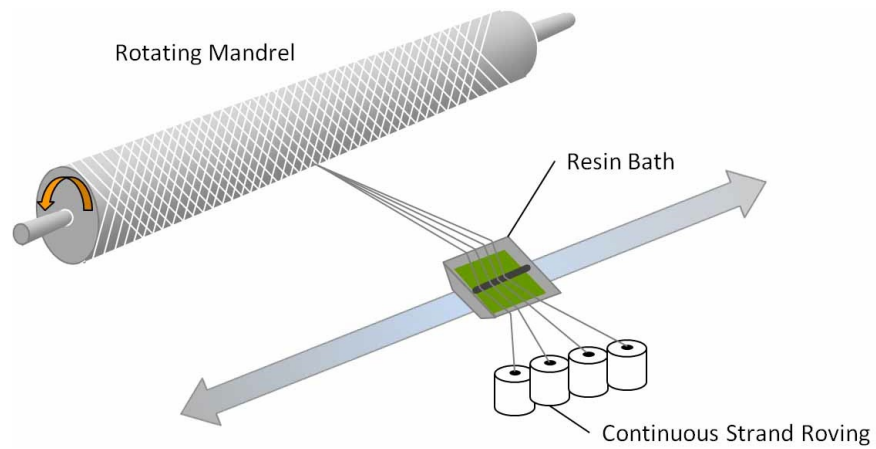


Figure 2.9: The process of filament winding. [50]

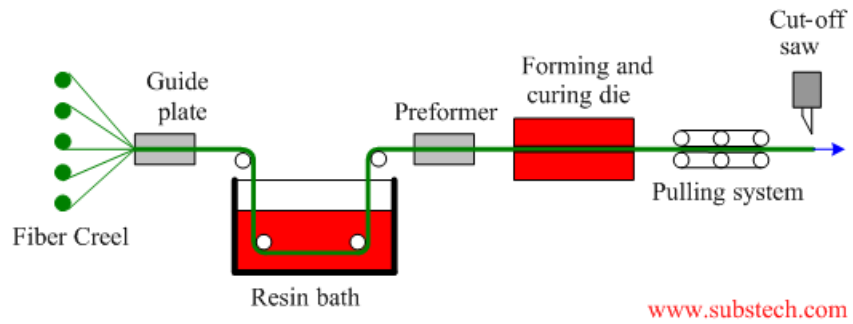


Figure 2.10: The process of pultrusion [54].

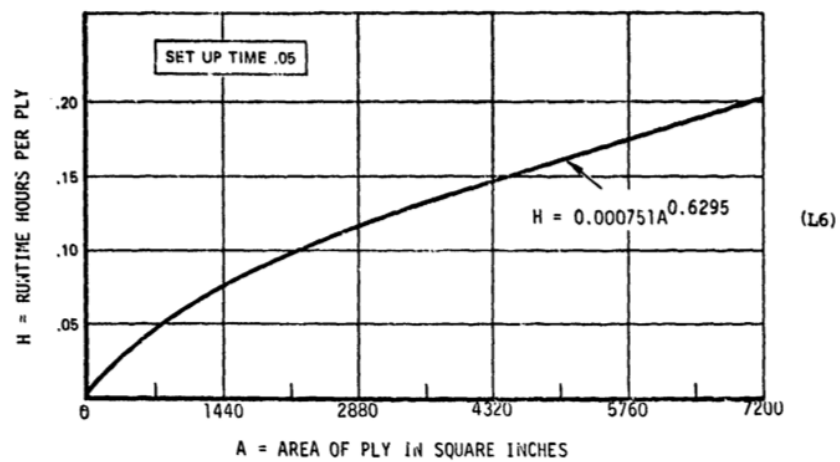


FIGURE 8. STANDARD EQUATION FOR  
MANUAL LAYUP OF WOVEN MATERIAL

Figure 2.11: Plot from Northrop study showing the time required to deposit woven fabric with respect to the area of a part.



Figure 2.12: Water jet created by a cavitation bubble imploding on a surface [76].

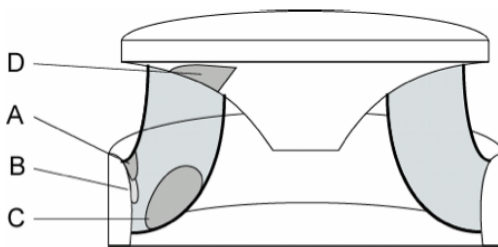


Figure 2.13: Common locations of cavitation erosion on a Francis runner. [77]

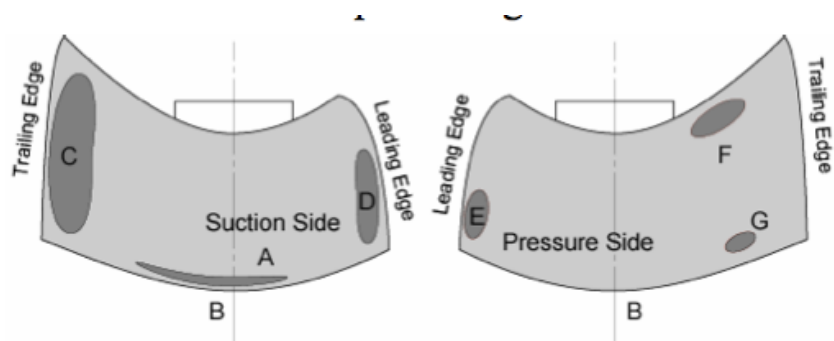


Figure 2.14: Common locations of cavitation erosion on a Kaplan runner blade. [77]

## Chapter 3: Materials and Methods

### 3.1 Component Design and Manufacturing

Two design case studies were completed to show the feasibility of composite turbine components over a range of designs; A 2 MW radial flow Francis machine and a 250 kW axial flow propeller machine. For each of these cases the following components are analyzed:

- Penstock
- Scroll Case (only relevant for the 2 MW case)
- Guide Vanes
- Runner
- Draft Tube
- Fish Ladder (modular and applicable to a range of facilities)

Each of these components by conventional materials is completed to provide a baseline and comparison. Designs are adjusted to accommodate composite materials while maintaining the original geometry as much as possible. Materials and methods of manufacture selected to minimize cost while providing adequate strength and

stiffness. A process and cost analysis following the methods described in section 2.4 is completed for the chosen manufacturing methods.

The 2 MW and 250 kW cases were chosen to be within the realm of small hydro, described as below 5 MW in Europe and 30 MW in the US [8, 9]. This is the realm where composites will have the most applicability in terms of overall machine size, required strength of the composite materials, and cost economy. Canyon Hydro graciously provided two designs with all the necessary parameters for building up models of the chosen components as shown in figures 3.2 and 3.1. The important sizing parameters for each turbine are noted alongside the parameters for the provided runner geometries in table 3.3.

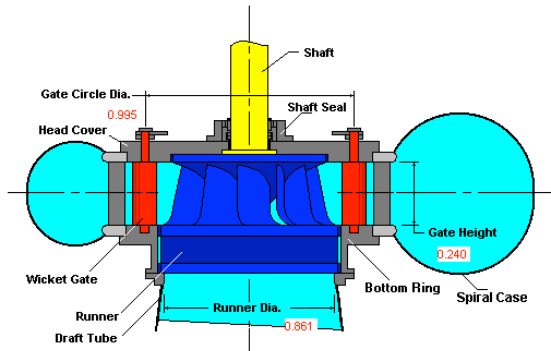


Figure 3.1: Model of the 2 MW Francis turbine.

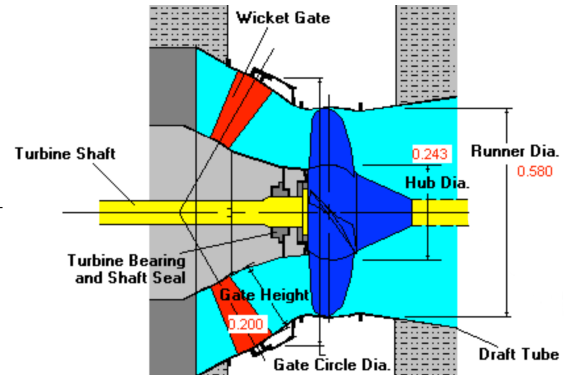


Figure 3.2: Model of the 250 kW propeller turbine.

### 3.1.1 Penstock

The penstock is a pipe and the steel reference design thickness was initially based on the hoop stress generated by the pressure head on the turbine for both models, which each had a diameter of 1.07 m. However, the required thickness was less than

that required by the Bureau of Reclamation and Pacific Gas and Electric installation and handling requirements for exposed penstocks [85]. The thicknesses for these requirements were calculated and the more conservative one, 6.35 mm was chosen as the design thickness.

Design criteria for the composite penstock were based on the net head pressure at the scroll case inlet and minimum thickness criteria as defined in [35]. These calculations were checked against commercially available FRP piping to ensure the validity of calculations for the penstock and the other components designed by this methodology; the draft tube and scroll case. The thickness determined by the hoop stress and installation and handling requirements was 23 mm.

The penstock is most easily manufactured using filament winding that is commonly used in the Fiber Reinforced Polymer (FRP) piping industry. The penstock requires 0°wraps, known as hoops, combined with helical 45°wraps to add strength in bending and handling. The price for manufacture was obtained from industry sources, as fiberglass piping is a well developed product commonly used in corrosive industrial environments. For comparison with other components, the cost of labor for the penstock was calculated using industry standards for filament winding as noted in [52].

### 3.1.2 Scroll Case

The scroll case directs the water through the guide vanes and onto the runner blades. A drawing with associated dimensions and an isometric view of the model used in

this design is presented in figures 3.3 and 3.4. The design of the steel scroll case was based on the maximum internal pressure, which is the pressure head created by the turbine. A safety factor of 2 was added to account for water hammer effects as is standard practice noted by [85]. However, as noted in section 3.1.1 the hydrostatic pressure load is much less than installation and handling thicknesses. It was determined that the scroll case would require similar thicknesses based on its also being a circular pressure vessel, the design thicknesses were based on the largest diameter of the casing at the inlet. Since this diameter is the same as the penstock, equivalent thicknesses were used for both components.

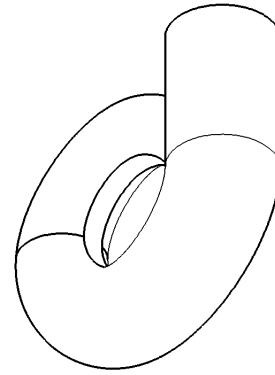
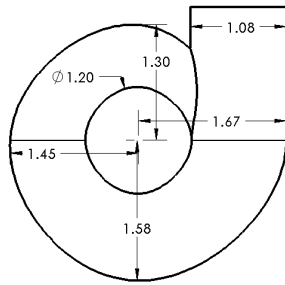


Figure 3.3: Drawing of the scroll case showing associated dimensions. Figure 3.4: Isometric drawing of the scroll case to clarify shape.

A safety factor of 15 was added in the composite design to account for water hammer and the design was based on the same internal pressure load as with the penstock. There was concern that the scroll case would want to unroll due to the open internal edge but this was allayed by noting that the top plate is held in place by the generator mounting structure and that the stay vanes are bonded to the upper and lower surfaces of the case near the inlet of the turbine. The calculated thickness

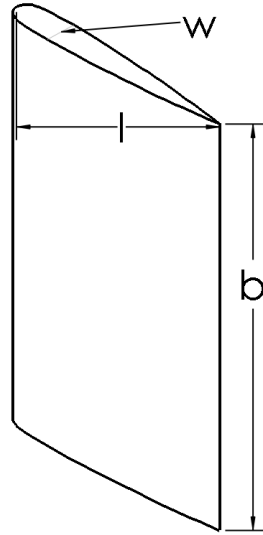
was 10 mm.

Hand layup and open mold vacuum infusion were selected as the methods of manufacture for the Scroll Case. These two methods were compared similar to the guide vane using two male molds to build each half of the structure with a secondary bonding step added to attach the two halves. For parts this large and complex, more automated methods such as compression molding require prohibitively large presses and tooling.

### 3.1.3 Guide Vanes

The basic form of a guide vane is a hydrofoil and in the interest of this design and feasibility study, we modeled the guide vane as a NACA 0015 airfoil, one of the most basic airfoil shapes from which many of the current designs are based. This provides a benchmark with which to compare the steel component to a composite design and this benchmark can be applied to situation specific hydrofoils with relative ease. The CAD model for the 2 *MW* and 250 *kW* guide vanes with associated dimensions is displayed in figure 3.5. Loading analysis of the vane was performed by calculating the lift and drag forces on the hydrofoil using Von Mises' formulae, which were applied to the gate as uniform distributed load along the span with the gate modeled as an asymmetric beam with an angle of attack of  $10.5^\circ$  [86]. See section 2.1 for a more in-depth derivation of this analysis.

The guide vanes are thick structures whose primary loading mode is bending. We therefore chose to design them with a sandwich structure, which puts a strong, stiff



	$l$ [m]	$b$ [m]	$w$ [m]
250 kW	.110	.200	.01
2 MW	.115	.240	.02

Figure 3.5: The guide vane model with relevant dimensions tabulated on the right.  $L$  and  $b$  are the total length and height of the vane and  $w$  is the width.

composite skin where the high bending stresses exist at the surface of the component and a lightweight core to provide shear strength. Both guide vanes were initially designed with a quasi-isotropic E-glass/Epoxy skin with a foam core. The 2 MW gate used a heavyweight fabric with an areal weight of  $1,350 \frac{g}{m^2}$  and the 250 kW gate used a mid weight  $690 \frac{g}{m^2}$  fabric. The core for both cases was made of a structural polypropylene foam.

Finite element (FE) analysis was first run with the vane modeled in steel with the gate fixed at the top and bottom. FE analysis allowed for a more accurate design given the complex geometry and loading scenario. The loading was applied to the surface using a quadratic pressure load based on the magnitude of the lift and drag forces applied over the surface of the vane. The total load was calculated by dividing the total load from the lift and drag forces by the height of the vane giving a distributed

line load; the same used in the beam analysis. This was integrated over chord length of the gate using a quadratic pressure distribution [87, 88, 89]. The method used is shown below in equation 3.1

$$w = \int_0^{l_v} Ay^2 dy = A \left( \frac{l_v^3}{3} \right) \Rightarrow A = w \frac{3}{l_v^3} \quad (3.1)$$

where  $w$  is the line load on the beam given by Von Mises formulae divided by the height of the beam,  $A$  is the pressure coefficient and  $l$  is the chord length of the vane in meters. The steel run provided a baseline comparison between the beam analysis and FE analysis. The resultant maximum deflection in the x-direction (normal to the beam axis) in the middle of the gate was 79.05% for the 2 *MW* FE model and 80.5% for the 250 *kW* FE model of the value obtained by the beam analysis, which was considered reasonable given the overly stiff boundary conditions applied in FE analysis. The model was then run with a possible 8-ply composite skin and the foam core mentioned above with the thickness based roughly off the maximum Von Mises stress. The FE results showed reasonable deflection and stress distributions. The FE analysis results for both models are presented in table 3.1. The maximum Von Mises stress for each gate is presented with the relative safety factor calculated from this value as the starting point for the design.

For anisotropic materials, the Von Mises failure criteria at best provides only a rough approximation of the stresses in the laminate. To ensure the strength of the vane, the Hashin damage criteria, as described in chapter 2 was applied to the model. The results of the criteria are shown below, calculated as described in section 2.3.

Component	$\Delta x [m]$	$\sigma_{max}[MPa]$	Rel. SF
Glass/Epoxy 2MW	1.240E-5	1.726E7	20
Glass/Epoxy 250kW	2.03E-5	1.459E7	24
Steel 2 MW	1.957E-6	1.159E7	72
Steel 250 kW	1.975E-6	1237E7	64

Table 3.1: Deflection, maximum Mises stress and relative safety factors for the Glass/Epoxy-Foam Core guide vane with comparisons for steel guide vanes.

The criteria is satisfied (damage is initiated) when the value is greater than 1. Table 3.2 shows the results for both cases. Both show that the layups are two or three orders of magnitude below failure in all modes, which accounts for the overestimation of strength in the Hashin criteria for combined shear and normal compressive loading [43].

	$F_f^t$	$F_f^c$	$F_m^t$	$F_m^c$
2 [MW]	3.38E-3	2.09E-3	3.46E-4	2.00E-4
250 [kW]	2.36E-5	1.370E-3	5.84E-4	3.71E-4

Table 3.2: Hashin damage criteria for tensile and compressive failure of the fiber and matrix for both guide vane models.

Two options were initially compared for the manufacturing of the guide vanes; VI and HLU. These were chosen based on their low equipment and labor costs respectively. Relative to other manufacturing methods, they are the lowest in terms of capital investment and provide the most accessible way to manufacture a small run of turbine components.

After the cost analysis (chapter 4) was completed, it was determined that the guide vane could possibly be manufactured more economically by a solid pultrusion.

However, the material response of the pultrusion material selected was anisotropic and determined to not have the necessary strength to manage varying load conditions within the turbine. It is likely that a pultrusion could be developed that could withstand the loads without a significant increase in price. Therefore, the cost of the pultrusion model is presented in chapter 4 along with the HLU and VI guide vanes.

### 3.1.4 Runner

Runner geometries for a Francis and Propeller machine were provided by Voith Hydro, images of the two complete geometries are shown in figure 2.3. As both of the Voith models were larger than the cases given by Canyon Hydro it was necessary to determine the validity of the runner geometry by comparing the specific speeds. Given the small difference relative to the range of values in which these turbine de-

	Francis		Propeller	
	Voith	2 [MW]	Voith	250 [kw]
$N$ [rps]	2.30	10.00	1.150	15.00
$Q$ [cms]	98.0	5.35	361.7	1.910
$H$ [m]	52.4	45.7	13.10	15.00
$P$ [W]	5.03E7	2.39E6	4.63E7	2.81E5
$N_s$	115.7	130.1	315	267
% diff.	11.72%		16.49%	

Table 3.3: Design parameters for the comparison of the blade profile between the Voith runner geometry and Canyon case studies.

signs are valid, as cited in section 2.1, the models were confirmed to be valid for the

smaller case studies. The blades for each case were scaled to match the size of units in the case studies and FE analysis was performed. The blades were fixed at the top and bottom edges as specified in the Canyon designs and a pressure load was applied to the surface to imitate the dynamic pressure load. This load was calculated using the machine power and speed as noted in section 2.1. where the  $L$  is the load in  $N$ ,  $P$  is the machine power in  $W$ ,  $N$  is speed in  $rpm$ ,  $n_b$  is the number of blades and  $r$  is the distance from the center of the shaft to the centroid of the blade in  $m$ . This load was applied over the blade using a quadratic pressure load distributed over the pressure side of the blade. For the runner, the distribution was based on the y-position relative to a datum coordinate system with the y-axis aligned to a meridional section in the middle of the blade. To obtain the pressure coefficient, the line load was calculated by dividing the total load by the average height of the blade. The integration to calculate the distributed load follow the same method used for the guide vanes in section 3.1.3 [88].

The load applied to the blade surface was compared to CFD work on hydroelectric turbines to confirm the validity of the pressure magnitude and profile [34, 90]. The analysis was run using the mechanical properties of steel and the the results were used as a benchmark to compare with the composite runner analysis. The pressure profile of the blade from this project's FEA analysis is shown next to the pressure profile from literature in figure 3.6. The figures show agreement in the distribution of loads, although the higher pressure is slightly more focused towards the front of the blade on the CFD model but the difference in load is less than 10% at any given

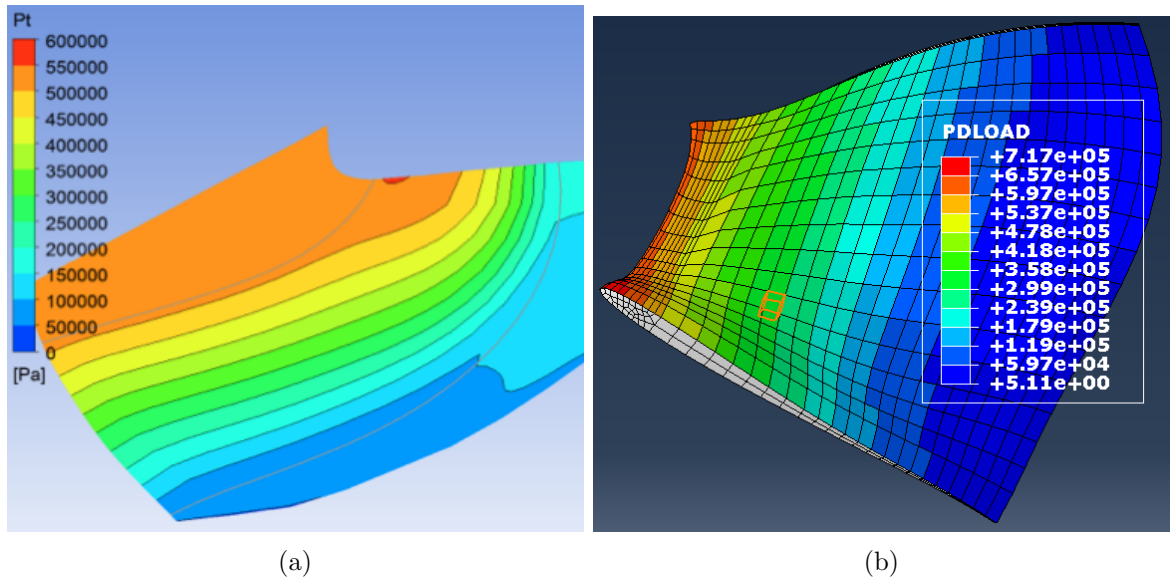


Figure 3.6: Comparison of a) CFD analysis of a Francis turbine blade and b) FEA analysis of a Francis blade from this project [34].

point along the surface of the blade. In addition to the pressure load, a centripetal rotational force was applied to the blade by inputting the density of the material and the provided rotational speed. The resulting centrifugal loads were applied to the blade in addition to the pressure load. In both cases the centrifugal loads reduced the stress created by the pressure load but the maximum Von Mises stress due to the inertial load was less than 10% of the pressure load at any given point.

Given the complexity of the blade, importing the blade into an FE program provided some challenges. To assist in the analysis a spline was added to the front edge of the blade, to split the geometry into the pressure and suction sides. Once the blade had been imported, further partitioning was needed to prevent highly distorted elements when meshing the blade. Two partitions were made using datum points on the

top and bottom edges of the blade as shown in figure 3.7. These partitions allowed the blade to be meshed with a more physically accurate C3D8R 8-node brick element instead of a pyramid shaped tetrahedron and with a smooth element distribution as shown in figure 3.8 for the Francis blade.

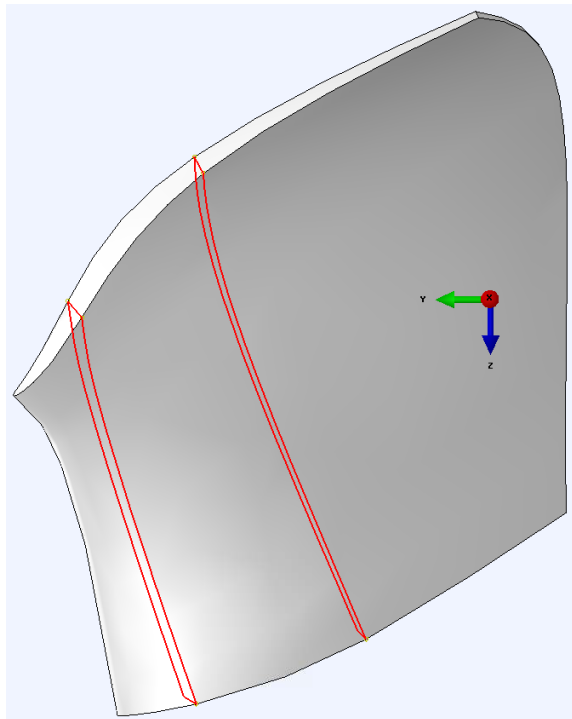


Figure 3.7: Partitions made on the runner blade to prevent distorted meshing.

With the model assumed to be valid, the material properties were changed to represent the Forged Composite material [49], which was modeled as an isotropic material given its random chopped prepreg reinforcement [51]. Analyses were run and the results showed high stresses at the fixed top edge. It was assumed that while these were relevant stress concentrations their magnitude was over estimated due to the overly stiff boundary conditions. FE analysis creates boundary conditions that fix

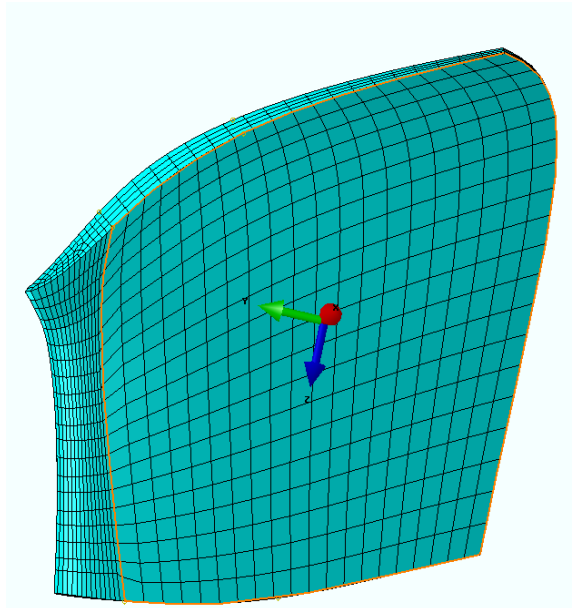


Figure 3.8: The mesh distribution allowed with the partitions.

an edge completely, allowing no movement at that point. In reality, a component will give slightly at these boundaries when it is loaded, reducing the stress concentration. The maximum Mises stress, maximum deflection and safety factor based on the Von Mises failure criteria given the isotropicity of the material are displayed in table 3.4. The deflection of both blades is around one millimeter, which will prevent them from

	2 [MW]	250 [kW]
Deflection [mm]	1.161	.8115
Max. Mises Stress [MPa]	1.358E8	2.24E8
Safety Factor	1.81	1.09

Table 3.4: FE blade model results.

striking the interior surfaces of the turbine casing. The safety factor of the Francis

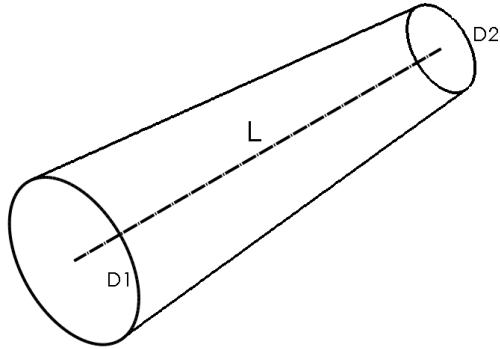
blade is reasonable considering that the airplane and space industries regularly apply safety factors of 1.4-1.5 to minimize weight when the properties of their components are well known and tested [91, 92]. However, some redesign of the propeller blade will need to occur to increase the safety factor above 1.4. It is assumed that these modifications would maintain the similar geometry (doubling the number of blades would halve the load per blade, doubling the safety factor) and so the manufacturing analysis was completed assuming the modifications would be made.

To manufacture the complex shape of the runner blade in a cost effective manner, the compression molding of a sheet molding compound (SMC) was selected. The mass of SMC required was calculated given the volume of the blade and the density of the compound.

Given the hydraulic validity of the steel model, the only changes made were the material properties. The composite turbine was designed using an isotropic randomly oriented carbon fiber prepreg sheet molding compound (SMC) as shown in figure 2.8. The tensile strength and modulus for the prepreg SMC are  $276 \text{ MPa}$  and  $62.1 \text{ MPa}$  respectively.

### 3.1.5 Draft Tube

The draft tube was modeled as a simple cylindrical diffuser, which is typical on medium sized turbine units. The CAD model of the draft tube with associated dimensions is displayed in 3.9.



	$D_1$ [m]	$D_2$ [m]	$L$ [m]
250 kW	.58	1.12	2.29
2 MW	.861	1.64	4.65

Table 3.5: Dimensions for both draft tube cases.

Figure 3.9: Draft tube with associated dimensions.

Steel design of the draft tube is based on the internal pressure  $p_2$ , actually a vacuum, at the discharge ring due to the suction created by the pressure head between the discharge ring and the tailrace (the open pool below the dam where the water exits the draft tube). The pressure at the top of the draft tube can be calculated using Bernoulli's equation.

The maximum pressure load (at the discharge ring), critical buckling loads, factor of safety and calculated thicknesses for the steel and composite draft tubes are compiled in table 3.6. The thicknesses for the steel draft tubes, 6 mm, were driven by the installation and handling criteria, as was the thickness for the 250 [kW] composite draft tube. Design for the composite draft tube was also based on the pressure load

	$P_{max}$ [MPa]	$P_{cr}$ [MPa]	SF	t [mm]
2 [MW]	-3.01E4	6.56E4	15	7
250 [kW]	-2.35E4	2.49E4	15	6

Table 3.6: Loads, chosen safety factor and calculated thickness for the composite draft tubes.

and beam stress for the draft tube and a safety factor of 15 was added, 10 is an industry standard for FRP piping, see [35] and this was increased by 1.5 to account for the use of natural fibers, whose properties and performance are less well known. A quasi-isotropic lay up was used to provide consistent strength for varying load conditions and this allowed the design process to follow the same method as for FRP piping and general isotropic materials.

Convex rotationally symmetric components are most efficiently and economically manufactured by filament winding, however this has not been commercially proven for use with natural fibers. To provide a realistic manufacturing plan, the chosen method was a wet layup of the flax fabric with a bio-based PLA resin on a flared mandrel. The labor costs were estimated using the Northrop model with adjustments for the added labor cost incurred by wet layup as noted in section 2.4. Tooling was estimated also using case studies completed for similar shapes [48].

### 3.1.6 Fish Ladder

Fish ladders are most frequently concrete structures, either free standing or attached to the dam structure. There are a number of different styles depending on the species of fish passing, the location and the variation of flow rate. For this project, a vertical slot ladder was chosen as it can function over a large range of flow rates as noted in [93]. The design is based off an example presented in [94] for a concrete fish ladder. A drawing of the fish ladder with dimensions is presented in figure 3.10.

This ladder was scaled to 50% of the dimensions noted above to accommodate

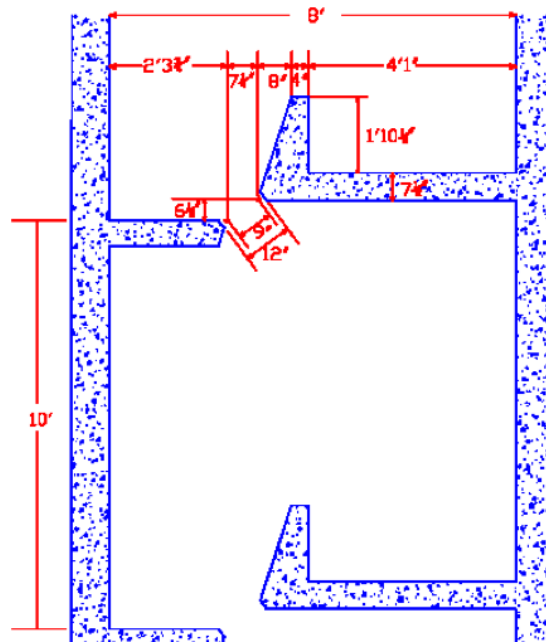


Figure 3.10: Vertical slot fish ladder used as a model for the composite fish ladder in this project (non-SI units from literature).

the smaller hydroelectric facilities studied in this project with the passage width maintained to provide adequate passage for large fish. However, the scaling does not imply that composites cannot be implemented into a full scale fish passage system.

For the composite model, design was based off the bending load on the largest area of wall subjected to a water load. This plate was modeled as being fixed on three edges and subject to a linearly increasing distributed load using equations from [24]. The maximum stress on the long wall of the C-section was  $1.00\text{E}7$  Pa for a thickness of 3 cm, which gives a factor of safety of 12 for a fiberglass spray [95].

$$\sigma_b = \frac{\beta qb^2}{t^2} \quad (3.2)$$

where  $\beta$  is a empirically derived coefficient,  $b$  is the height of the plate and the wall thickness was chosen to be  $t = 0.03$  to ensure strength. Assuming bending dominates, the maximum stress failure criteria was applied with the material being a Glass/Polyester spray up composite with a tensile strength of  $50.2E6 \text{ MPa}$  as noted by [96]. The interior sections are a natural fiber pultrusion material with similar properties, as noted by [67, 97], so the loading on the larger C-section panels are the limiting design criteria.

The fish ladder is made from a combination of pultrusion for the interior profiles and spray up for the exterior c-section as noted in 3.11. In the case of the fish ladder, the spray up will be done on a male C-section mold. Once the C-section has been cured, the flanges will be machined into the top and bottom edges and the profiles will be bonded to the interior surface.

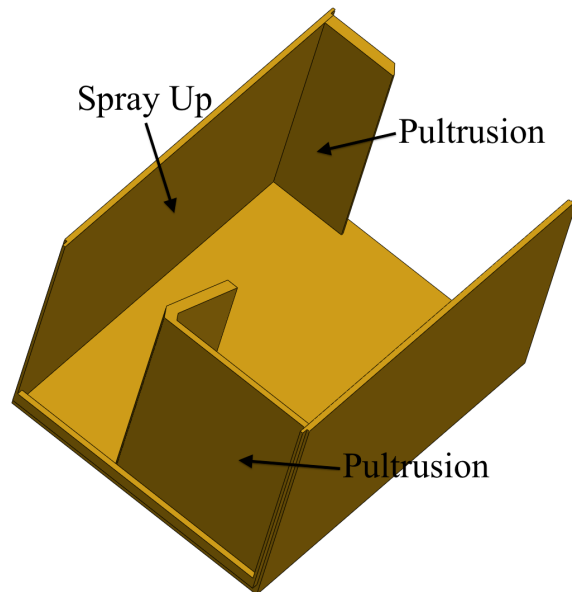


Figure 3.11: Image highlighting the different parts of the fish ladder and their associated manufacturing techniques.

## Chapter 4: Results and Discussion

### 4.1 Manufacturing Process Results

A summary of the manufacturing process with associated labor hours and tooling requirements for the two turbine cases are given in tables 4.1 and 4.2. For the hand lay up and vacuum infusion models the fiber loading was assumed to be 50% by weight, the spray up was assumed to be 40% and the SMC was 53% [49].

<b>Component</b>	<b>Method</b>	<b>A [<math>m^2</math>]</b>	<b>Wt. [<math>kg</math>]</b>	<b>Labor [<math>hrs</math>]</b>	<b>Tooling</b>
Runner	SMC	3.91	33.9	5.89	Closed Mold
Guide Vanes (20)	VI	1.372	36.2	6.44	Female mold
	HLU			11.86	
Draft Tube	HLU	18.33	213	67.9	Mandrel
Scroll Case	VI	19.84	1342	70.1	2 x Male Mold
	HLU			450	
Penstock	Fil. Winding	3.36/ $m$	120/ $m$	17.45	Mandrel

Table 4.1: Summary of the manufacturing parameters for the 2 [MW] turbine case.

<b>Component</b>	<b>Method</b>	<b>A [<math>m^2</math>]</b>	<b>Wt. [<math>kg</math>]</b>	<b>Labor [<math>hrs</math>]</b>	<b>Tooling</b>
Runner	SMC	1.204	20.8	1.119	Closed Mold
Guide Vanes (20)	VI	0.987	14.37	5.25	Female mold
	HLU			7.27	
Draft Tube	HLU	7.79	90.4	30.5	Mandrel
Penstock	Fil. Winding	3.36/ $m$	120/ $m$	17.45	Mandrel
Fish Ladder	Spray / Pult.	4.76	156.1	7.81	Male mold

Table 4.2: Summary of the manufacturing parameters for the 250 [kW] turbine case.

It is clear from the tables that vacuum infusion is the preferred method for manufacturing the guide vanes and especially the scroll case as the lay up and wetting of the fabric is 95.7% of the total time, making the labor prohibitively high. The investment in a vacuum pump and other peripherals would quickly be returned over the course of a small number of parts and would make the overall manufacturing process much more economical.

While the draft tube was chosen to be manufactured by hand lay up in this project, it will see a two-thirds reduction in labor time when the filament winding of natural fibers is commercialized. The process can deposit up to 9 *kg* an hour, which would allow the component to be manufactured in 23.7 hours as opposed to 67.9. And while this study assumed equal resin use for both hand lay up and vacuum infusion, the latter allows for higher fiber weight percentages ( 50%), which optimizes the quality, lowers void content and increases strength, of parts with a lower overall material cost.

The fish ladder was added to table 4.1 for convenience but it could be associated with either model. Pultrusion was also considered as a possible method of manufacture but the large size makes the cost of the die over \$200,000; only economical at very high production rates when compared with a sheet metal male spray up mold as tabulated in table 4.3.

The weights of all the above components were calculated and compared with current steel designs as noted in tables 4.3 and 4.4 below.

<b>Component</b>	<b>Composite Wt. [kg]</b>	<b>Steel wt. [kg]</b>	<b>Percent diff.</b>
Penstock	120 /m	167.1 /m	71.8%
Guide Vanes	36.2	64.5	56.1%
Draft Tube	213	797	26.7%
Runner	33.9	185	18.32%
Scroll Case	1342	1392	96.4%
<b>Totals</b>	<b>7016</b>	<b>9888</b>	<b>70.9%</b>

Table 4.3: Weight differences between steel and composite components on a 2 MW Francis machine.

<b>Component</b>	<b>Composite Wt. [kg]</b>	<b>Steel wt. [kg]</b>	<b>Percent diff.</b>
Penstock	120/m	167 /m	71.9%
Guide Vanes	14.4	37.4	38.5%
Draft Tube	90.4	257	35.2%
Runner	20.8	117	17.78%
Fish Ladder (no total)	213	1500	14.20%
<b>Totals</b>	<b>1927</b>	<b>3734</b>	<b>51.6%</b>

Table 4.4: Weight differences between steel and composite components on a 250 kW propeller machine.

## 4.2 Cost Models

Using the labor and equipment information from section 4.1, the costs associated with the manufacture of each part were calculated. For simplicity, the results for the components in each turbine are tabulated in figures 4.1 and 4.2 broken down by materials and labor. Material costs include the fibers, either fabric, rovings or SMC, resin, gel coat and plastics needed for VI, costs were taken from sources in industry and literature. The cost of the guide vanes represents 20 vanes, which is enough for a small machine and the cost of the penstock is based on the head of the turbine,

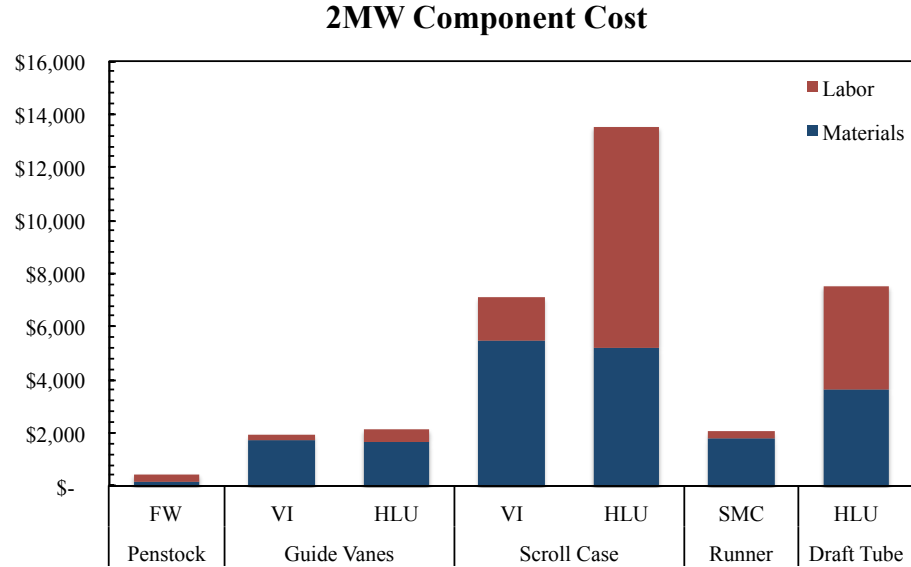


Figure 4.1: Cost of materials and labor for the 2MW turbine components.

45 m for the 2 MW case and 15 m for the 250 kW case. While it is possible that a longer penstock could be required depending on the site this allows for a more realistic comparison between components. The cost per meter of penstock along with the labor, materials, tooling and totals for the other components are also presented in table form in tables 5 and 6 in the appendix.

The tooling costs shown in figure 4.3 for the complete manufacture and preparation of the tool including design; the totals for each component assume a small run of 10 parts. This represents the volume that would likely be manufactured in a testing scenario and the price per part would drop significantly if the machines went into full scale production. The type of tooling and associated longevity are discussed in the following sections along with a discussion of the final costs and possible alternatives.

The runner mold, based on the model presented in [63] is designed to be used for

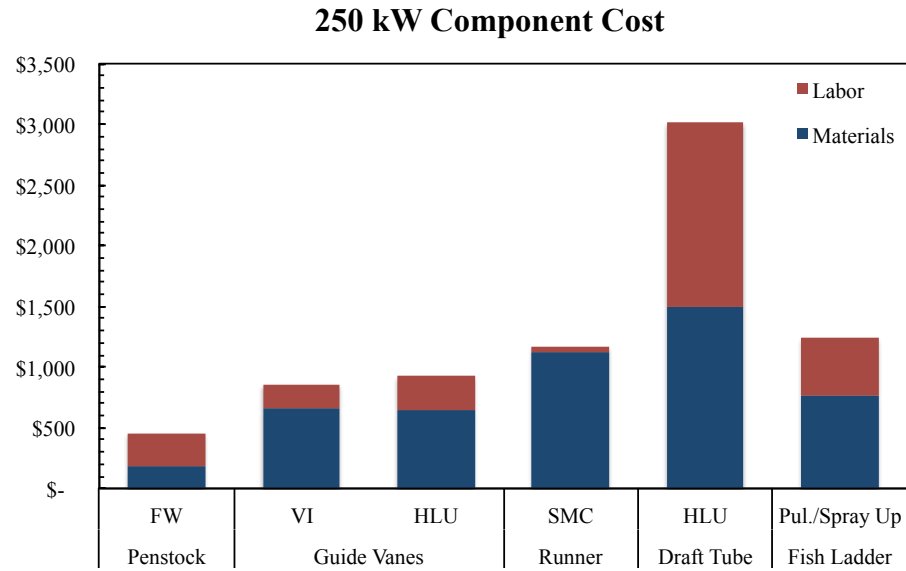


Figure 4.2: Cost of materials and labor for the 250kW turbine components.

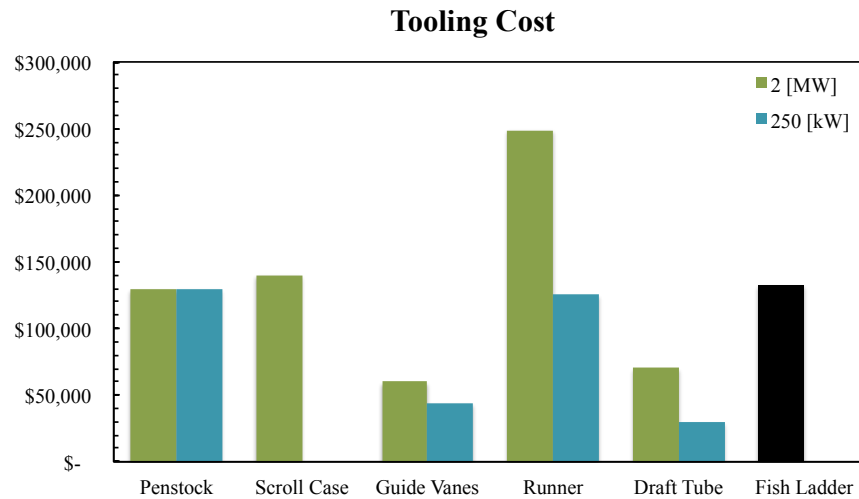


Figure 4.3: Costs of tooling for the 2MW turbine components.

up to 50,000 parts. The same is true for the guide vanes, draft tube, penstock and scroll case molds. The fish ladder spray up mold is of lower quality given the lower tolerances on surface roughness and general profile, it is based on a quote for a run of closer to 1,000 parts. The pultrusion die costs were originally calculated based on work in [48] but there was concern that the scaling for the fish ladder parts was not accurate as the dies were quoted at \$300,000 and \$600,000 for the 250 [kW] and 2 [MW] models, respectively. A case study completed by [98] cited the cost of a die for a part closer to the cross-sectional area of the fish ladder sections. This study produced more reasonable scaled costs and was considered reasonable given the high complexity of the part produced - a bridge floor section with multiple cavities.

The difference in labor times for HLU as compared to VI noted in the manufacturing process results is even more clear in the overall costs with the labor costs 60% of combined cost for hand lay up of the scroll case while labor is 20% of the combined cost for the same component produced by vacuum infusion. The difference is less pronounced with the guide vanes, where the material are twice the cost of the labor for VI and the overall cost is dominated by the tooling. For a run of 30 machines, the cost of the gate would be half as much, \$3,398.30 and the difference between the two methods would become significant. The tooling also dominates the cost of the draft tube, especially as the materials, flax fiber from [60] and PLA resin from [70] are much less expensive than synthetic glass and polyester.

Total cost for a 10 part run with the total tooling cost divided amongst the 10 parts are presented in 4.4 for both machines and the fish ladder. The scroll case costs

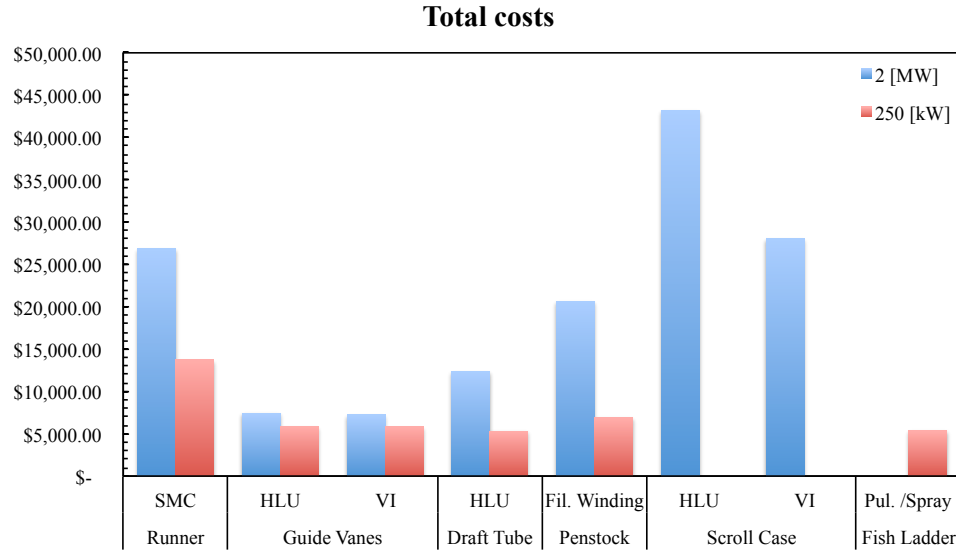


Figure 4.4: Total cost for manufacture of components from both turbine cases.

the most due to its complex geometry, size and the need to perform a secondary bond on the two halves together. As noted in table 3, the majority of the cost is due to the lay up of the fabric for HLU. The graph in figure 4.1 illustrates how the labor dominates the cost of the scroll case for that method of manufacture. VI reduces this total cost to be closer to the cost of the runner, a smaller but more complex component.

## Chapter 5: Conclusion

### 5.1 Feasibility results

The above work has shown that it is feasible to manufacture turbines from composite components. The components analyzed were the runner, guide vanes, draft tube, penstock for a 2 *MW* radial flow Francis machine and a 250 *kW* axial flow propeller machine. Additionally, the project includes the scroll case of the Francis machine and the design of a composite fish ladder to show the application of composites to other aspects of hydroelectric facilities. Composite design was based on current steel designs and modifications were made to accommodate composite design and manufacture while maintaining the original geometry as much as possible. Glass fabric was the dominant material, used in the guide vanes, scroll case, penstock and fish ladder exterior walls for its good strength and low cost. A chopped carbon fiber prepreg was used for the runner as it allowed for the compression molding of the complex blade, hub and band shapes. Natural fibers were used in the manufacture of the draft tube and interior sections of the fish ladder.

There is a general trend of tooling dominating the costs and this is expected for a short run of ten parts as one of the benefits of using composites as opposed to steel is the economy of scale gained by the reusable tooling, especially in the automated methods such as compression molding and pultrusion. While this project does show

the technical feasibility of using composites in hydroelectric turbines, the economic feasibility will come with the demand for machines that can be easily installed in remote areas with low maintenance requirements and, as natural and recycled fibers are further integrated into commercial processes, reduced environmental impact in manufacture and end of life.

The difference in material cost for natural fibers with their high specific properties makes them attractive. For example, the draft tube for the 2 *MW* model in this study weighs 39.6% of a comparable steel component, which is a 10% reduction from the weight of a glass fabric based component. The material cost is similar to glass fabric of similar weight. The original purpose of using natural fibers is the reduction in environmental pollution, which has been confirmed in studies comparing the total manufacturing and material usages between the two processes.

The difference in weight is even more pronounced for the fish ladder, which weighs 14.2% of the equivalent concrete structure, which is primarily due to the high specific properties of the composites compared to concrete. However, the total cost of \$5,352.99 not including the cost of install, is prohibitively expensive as the material and labor cost of a concrete ladder of the same size would cost roughly \$1,046.99. However, this does not include the cost of transporting the concrete, form material and rebar to the location. For a remote location, this can bring the two totals much closer together.

## Chapter 6: Future Work

Future work is needed to address further development of automated manufacturing methods to include natural fibers. As noted in the example of manufacturing the draft tube by filament winding, this will significantly reduce labor costs while taking advantage of the lower density and environmental impact of natural fibers. These advances will allow natural fiber composites to be competitive economically with current designs that use steel and concrete.

With natural fibers becoming a key component in the composite market, further testing is necessary to determine the operational life of these components. It is well known that environmental factors, such as hygroscopy and UV light, degrade synthetic fibers and initial work has shown that natural fibers suffer as much or more from these and other environmental factors. To ensure the components function well and have a lifetime that allows for a return on the investment, more research into the service life of these materials is needed.

In addition to manufacturing changes, there are structural concerns that still require further testing. While cavitation can be minimized by operating turbines within their design parameters there will always be times when the unit is outside of normal conditions and damage can occur. To know the extent of this damage, testing needs to be conducted on composite turbines and the necessary preventative measures, coatings or otherwise, need to be implemented to ensure the longevity of

the units; especially if they are to be installed in remote locations where maintenance cannot occur on a regular basis.

## Bibliography

- [1] J. B. Francis, *Hydraulic Experiments*. D. Van Nostrand, 192 Broadway. London: Trubner & Co., 1868.
- [2] E. T. Layon, *From Rule of Thumb to Scientific Engineering: James B. Francis and the Invention of the Francis Turbine.* NLA Monograph Series. Stony Brook, 1992.
- [3] Z.-y. Mei, *Mechanical Design and Manufacturing of Hydraulic Machinery*. Avebury, 1991.
- [4] U. S. A. C. of Engineers, “Bonneville Dam and Lock Brochure,” Technical Report.
- [5] “Grand Coulee Dam Fact Sheet.” [Online]. Available: <http://www.usbr.gov/pn/grandcoulee/pubs/factsheet.pdf>
- [6] K. Alanne and A. Saari, “Distributed energy generation and sustainable development,” *Renewable and Sustainable Energy Reviews*, vol. 10, pp. 539–558, 2006.
- [7] Report shows potential for global small hydro growth, development. [Online]. Available: <http://www.hydroworld.com/articles/2012/07/report-shows-potential-for-global-small-hydro-growth-development.html>
- [8] “Strategic study for the development of small hydro in the European Union,” European Small Hydro Association, Tech. Rep., 2010.
- [9] H. R. F. National Hydropower Association, Oak Ridge National Laboratory, “Summary report,” in *Summit Meeting*, 2010.
- [10] K. M. Kibler and D. D. Tullos, “Cumulative biophysical impact of small and large hydropower development in Nu River, China,” *Water Resources Research*, pp. n/a–n/a, 2013. [Online]. Available: <http://dx.doi.org/10.1002/wrcr.20243>
- [11] Int Pow: Norwegian Renewable Energy Partners, “World hydro potential and developments,” 2009.

- [12] D. Roach, K. Rackow, and W. Delong, “In-situ repair of steel bridges using advanced composite materials,” in *Proceedings of the Transportation Research Circular*, 2008, pp. 269–285.
- [13] F. Britt, “Stainless steel vs. fiberglass pipe,” *Chemical Engineering*, vol. 97, pp. 105–108, 1990.
- [14] D. Elliot and R. Trask, “Damage tolerance and repair of gfrp warships,” *Journal of Thermoplastic Composite Materials*, vol. 14, pp. 201–212, 2001.
- [15] S. Joshi, L. Drzal, A. Mohanty, and S. Arora, “Are natural fiber composites environmentally superior to glass fiber reinforced composites?” *Composites: Part A*, vol. 35, pp. 371–376, 2004.
- [16] F. M. White, *Fluid Mechanics*. Mc Graw Hill, 2003.
- [17] M. F. Ashby, *Material Selection in Mechanical Design*. Elsevier, 2011.
- [18] R. Turton, *Principles of Turbomachinery*. E & F N. Spon Ltd., 1984.
- [19] G. Krivchenko, *Hydraulic Machines: Turbines and Pumps*. Lewis Publishers, 1994.
- [20] Image of the scoll case in a radial flow machine. [Online]. Available: <http://photos.tradeholding.com/>
- [21] H. C. R. Krishna, Ed., *Hydraulic Design of Hydraulic Machinery*. Avebury, 1997.
- [22] R. V. Mises, *Theory of Flight*. Dover, 1959.
- [23] A. P. Boresi and R. J. Schmidt, *Advanced Mechanics of Materials*. John Wiley and Sons, 2003.
- [24] W. C. Young and R. G. Budynas, *Roark’s Formulas for Stress and Strain*. McGraw-Hill, 2002.
- [25] “Runner designs provided by Voith Hydro,” July 2012.
- [26] “(personal communication). Charlie Allen, Sr. Mechanical Engineering, United States Army Corps of Engineers - Hydro Design Center,” June 2012.

- [27] J. Gordon, "Hydraulic turbine efficiency," *Canadian Journal of Civil Engineering*, vol. 28, pp. 238–253, 2001.
- [28] J. Meriam, *Engineering Mechanics Volume 1: Statics*. John Wiley and Sons, 1978.
- [29] C. P. Kothandaraman and R. Rudramoorthy, *Fluid Mechancis and Machinery*. New Academic Science, 2011.
- [30] "Image of blade profiles for given runner specific speeds," 2013. [Online]. Available: [http://www.power-eng.com/content/dam/etc/medialib/power-engineering/april/7630.res/\\_jcr\\_content/renditions/pennwell.web.600.305.gif](http://www.power-eng.com/content/dam/etc/medialib/power-engineering/april/7630.res/_jcr_content/renditions/pennwell.web.600.305.gif)
- [31] H. G. Allen, *Background To Buckling*. McGraw-Hill; United Kingdom, 1980.
- [32] D. Grogan, S. Leen, C. Kennedy, and B. , "Design of composte tidal turbine blades," *Renewable Energy*, vol. 57, pp. 151–162, 2013.
- [33] J. Wang and N. Mller, "Numerical investigation on composite material marine current turbine using cfd," *Central European Journal of Engineering*, vol. 1(4), pp. 334–340, 2011.
- [34] F. Ayancik, U. Aradag, E. Ozkaya, K. Celebioglu, O. Unver, and S. Aradag, "Hydroturbine runner design and manufacturing," *International Journal of Materials, Mechanics and Manufacturing*, vol. 1, pp. 162–165, 2013.
- [35] , "FRP Design Manual," Reinforced Plastic Systems Inc., Tech. Rep., 2006.
- [36] Multiple, "Design manual," Reinforced Plastic Systems, Tech. Rep., 2006.
- [37] I. M. Daniel and O. Ishai, *Engineering Mechanics of Composite Materials*. Oxford University Press, 2006.
- [38] B. A. Strong, *Fundamentals of Composites Manufacturing*. Society of Manufacturing Engineers, 2008.
- [39] R. L. Hankinson, "Investigation of the curshing strength of spruce at varying angles of grain," *Air Service Information Circular No.259 U.S. Air Services*, 1921.
- [40] Z. Hashin, "Failure criteria for unidirectional fiber composites," *Journal of Applied Mechanics*, vol. 47, pp. 329–334, 1980.

- [41] M. Tsai, Stephen and E. M. Wu, "A general theory of strength for anisotropic materials," *Journal of Composite Materials*, vol. 5, pp. 58–80, 1971.
- [42] P. Clouston, "The tsai-wu strength theory for douglas-fir laminated veneer," Ph.D. dissertation, The University of British Columbia, 1989.
- [43] M. Hinton, A. Kaddour, and P. Soden, "A comparison of the predictive capabilities of current failure theories for composite laminates, judged against experimental evidence," *Composites Science and Technology*, vol. 62, pp. 1725–1797, 2002.
- [44] P. Soden, M. J. Hinton, and A. Kaddour, "A comparison of the predictive capabilities of current failure theories for composite laminates," *Composite Science and Technology*, vol. 58, pp. 1225–1254, 1998.
- [45] An image showing the vacuum infusion process. [Online]. Available: <http://www.carbonbydesign.com/images/vip.png>
- [46] The wet lay up process. [Online]. Available: <http://www.carbonfiberguru.com/wp-content/uploads/2010/01/Hand-Lay-up.jpg>
- [47] S. K. Mazumdar, *Composites Manufacturing: Materials, Product and Process*. CRC Press, 2002.
- [48] S. M. Hafner, "Cost modeling and design for manufacturing guidelines for advanced composite fabrication," Ph.D. dissertation, Massachusetts Institute of Technology, 2002.
- [49] Q. Composites, "AMC<sup>®</sup> 8590 Engineered Structural Composite (ESC<sup>®</sup>) Molding Compound," November 2012. [Online]. Available: <http://www.quantumcomposites.com/products/amc/>
- [50] [Online]. Available: <http://www.moldedfiberglass.com/processes/filament-winding-process>
- [51] P. Feraboli, E. Peitso, and T. Cleveland, "Modulus measurement for prepreg-based discontinuous carbon fiber/epoxy systems," *Journal of Composite Materials*, vol. 43, pp. 1947–1965, 2009.

- [52] F. W. DuVall, "Cost Comparisons of Wet Filament Winding Versus Prepreg Filament Winding for Type II and Type IV CNG cyclinders," Cordant Technologies, Tech. Rep., 2000.
- [53] T. F. Starr, Ed., *Pultrusion for Engineers*. CRC Press, 2000.
- [54] Pultrusion process schematic. [Online]. Available: <http://www.substech.com/>
- [55] D. J. LeBlanc, *Advanced Composite Cost Estimating Manual (on p.28)*, Northrop Corporation, August 1976.
- [56] M. Tse, "Design cost model for advanced composite structures," Master's thesis, Massachusetts Institute of Technology, September 1992.
- [57] G. Composites, "Wind energy handbook - chapter 6: Comparitive cost study of infusion versus hand lay-up," 2013.
- [58] *Optimization of Large Composite Structures Using Vacuum Infusion Simulation Techniques*. Composites Consulting Group, 2012.
- [59] J. L. Clarke, Ed., *Structural Design of Polymer Composites: EUROCOMP Design Code and Handbook*. Chapman & Hall, 1996.
- [60] "Price quote on Biotex Flax Fabric," Composites Evolution, May 2013.
- [61] J. V. Busch, "Primary fabrication methods and costs in polymer processing for automotive applications," Master's thesis, Massachusetts Institute of Technology, 1983.
- [62] J. Busch, "Micro-Computer Based Cost Estimation for the SMC Process," created as part of masters thesis.
- [63] G. Boothroyd, P. Dewhurst, and W. A. Knight, *Product Design for Manufacture and Assembly*. CRC Press, 2001.
- [64] F. T. Wallenberger and N. Weston, *Natural Fibers, Plastics and Composites*. Kluwer Academic Publishers, 2004.
- [65] B. C. S. FIMMM, Ed., *Industrial Fibers: Recent and Current Developments*, 2009.
- [66] Lotus Eco Elise. [Online]. Available: <http://www.lotuscars.com/gb/engineering/eco-elise>

- [67] I. Angelov, S. Wiedmer, M. Evstatiev, K. Friedrich, and G. Mennig, "Pultrusion of flax/polypropylene yarn," *Composites Part A*, vol. 38, pp. 1431–1438, 2007.
- [68] Thomas technik - natural fiber pultrusions. [Online]. Available: <http://www.thomas-technik.com/pultrusion.htm>
- [69] P. Lehtiniemi, K. Dufva, T. Berg, M. Skrifvars, and P. Jrvell, "Natural fiber-based reinforcements in epoxy composites processed by filament winding," *Journal of Reinforced Plastics and Composites*, vol. 30(23), pp. 1947–1955, 2011.
- [70] K. L. Pickering, Ed., *Properties and Performance of Natural-Fiber Composites*. CRC Press, 2008.
- [71] M. A. Fuqua, H. Shanshan, and C. A. Ulven, "Natural fiber reinforced composites," *Polymer Reviews*, vol. 52, pp. 259–320, 2012.
- [72] J. Almeida, "Analysis of cost and flexural strength performance of natural fiber-polyester composites," *Polymer-plastics technology and engineering*, vol. 40, pp. 205–215, 2001.
- [73] J. George, M. Sreekala, and S. Thomas, "A review of interface modification and characterization of natural fiber reinforced plastic composites," *Polymer Engineering and Science*, vol. 41, pp. 1471–1485, 2001.
- [74] K. Oksman, M. Skrifvars, and J.-F. Selin, "Natural fibres as reinforcements in polylactic acid (pla) composites," *Composites Science and Technology*, vol. 63, pp. 1317–1324, 2003.
- [75] P. Kumar and R. Saini, "Study of cavitation in hydro turbines - a review," *Renewable and Sustainable Energy Reviews*, vol. 14, pp. 374–383, 2010.
- [76] P. Robinson, B. J. R., T. Kodama, A. Shima, and Y. Tomita, "Interaction of cavitation bubbles with a free surface," *Journal of Applied Physics*, vol. 89, pp. 8225–8237, 2001.
- [77] F. Avellan, "Introduction to cavitation in hydraulic machinery," in *The 6th International Conference on Hydraulic Machinery and Hydrodynamics*, 2004.
- [78] K. H. Light, "Development of a cavitation erosion resistant advanced material system," Master's thesis, University of Maine, 2005.

- [79] R. Sollars and A. D. Beitelman, “Cavitation-resistant coatings for hydropower turbines,” United States Army Corps of Engineers, Tech. Rep., 2011.
- [80] J. Abot, Y. A., and I. Daniel, “Hygroscopic behavior of woven fabric carbon-epoxy composites,” *Journal of Reinforced Plastics and Composites*, vol. 24, pp. 195–207, 2005.
- [81] H. Choi, K. Ahn, J. Nam, and C. H.J., “Hygroscopic aspects of carbon/expoy fiber composite laminates in aircraft environments,” *Composites: Part A*, vol. 32, pp. 709–720, 2001.
- [82] D. Spurr, *Heart of Glass: Fiberglass Boats and the Men Who Build Them*. International Marine/Ragged Mountain Press, 1999.
- [83] E. Greene, *Marine Composites*. Eric Greene Associates, 1999.
- [84] H. M. Akil, L. W. Cheng, Z. M. Ishak, A. A. Bakar, and M. A. Rahman, “Water absorption study on pultruded jute fibre reinforced unsaturated polyester composites,” *Composites Science and Technology*, vol. 69, pp. 1942 – 1948, 2009.
- [85] *Steel Penstocks*, ASCE Std.
- [86] O. Antonsen, “Usteady flow in wicket gate and runner with focus on static and dynamic load on runner,” Ph.D. dissertation, Norweigian University of Science and Technology, 2007.
- [87] A. C. Ugural, *Mechanics of Materials*. John Wiley and Sons, 2008.
- [88] M. K. Shukla, R. Jain, V. Prasad, and S. Shukla, “CFD Analysis of 3-D Flow for Francis Turbine,” *MIT International Journal of Mechancial Engineering*, vol. 1, pp. 93–100, 2011.
- [89] R. Gong, H. Wang, Y. Yao, L. Shu, and Y. Huang, “Numerical Simluation of Pressure Fluctuation in 1000MW Francis Turbine Under Small Opening Condition,” in *26th IAHR Symposium on Hydraulic Machinery and Systems*, 2012.
- [90] Z. Carija, Z. Mrsa, and F. Sanjin, “Validation of Francis Water Turbine CFD Simulations,” *Strojarstvo*, vol. 50, pp. 5–14, 2008.

- [91] *Structural Design and Test Factors of Safety For Spaceflight Hardware*, National Aeronautics and Space Administration Std.
- [92] A. Kale, E. Acar, and R. T. Haftka, “Why are airplanes so safe structurally? effect of various safety measures on structural safety of aircraft,” in *Structures, Dynamics and Materials Conference*, 2004.
- [93] “Fish passage technologies: protection at hydropower facilities,” Congress of the United States, Washington D.C., Tech. Rep., September 1995.
- [94] B. P. Nordlund, “Design of upstream fish passage systems,” National Marine Fisheries Service, NWR, Tech. Rep., June 2009.
- [95] B. J. Pope, “Spray deposition of cork reinforced polyester,” Master’s thesis, Massachusetts Institute of Technology, 2010.
- [96] G. Designs. CES EduPack 2012.
- [97] K. Van De Velde and P. Kiekens, “Thermoplastic pultrusion of natural fibre reinforced composites,” *Composite Structures*, vol. 54, pp. 355–360, 2001.
- [98] T. B. Patrawala, “Decision support tool for costing of the pultrusion process,” Master’s thesis, West Virginia University, 1999.

## APPENDICES

Process	person-hours	
	Vacuum Infusion	Hand Lay Up
Clean Tool	0.063	0.063
Apply Release Agent	0.069	0.069
Gel Coat	0.069	0.069
Cut Plies and Plastics	0.468	0.340
Lay Up Fabric	0.797	8.598
Cut Core	0.392	0.392
Vacuum Bag	1.472	-
Infusion	0.5	-
Secondary Bonding	0.306	0.306
Demold	0.539	0.252
Finishing	1.770	1.770
<b>Totals</b>	<b>6.446</b>	<b>11.860</b>

Table 1: Process model and person-hours for hand layup and vacuum infusion manufacturing methods for 2 MW wicket gate [55].

Process	person-hours	
	Vacuum Infusion	Hand Lay Up
Clean Tool	0.059	0.059
Apply Release Agent	0.064	0.064
Gel Coat	0.064	0.064
Cut Plies and Plastics	0.465	0.338
Lay Up Fabric	0.657	0.306
Cut Core	0.306	4.236
Vacuum Bag	1.200	-
Infusion	0.500	-
Secondary Bonding	0.238	0.238
Demold	0.431	0.202
Finishing	1.762	1.762
<b>Totals</b>	<b>5.245</b>	<b>7.268</b>

Table 2: Process model and person-hours for hand layup and vacuum infusion manufacturing methods for 250 *kW* wicket gate [55].

Process	person-hours	
	Vacuum Infusion	Hand Lay Up
Clean Tool	0.240	.240
Apply Release Agent	0.335	.335
Gel Coat	0.335	.335
Cut Plies and Plastics	1.682	1.459
Lay Up Fabric	47.4	431
Vacuum Bag	6.33	-
Infusion	1.000	-
Secondary Bonding	2.38	8.05
Demold	8.05	2.38
Finishing	2.45	2.45
<b>Totals</b>	<b>70.1</b>	<b>450</b>

Table 3: Process model and person-hours for hand layup and vacuum infusion manufacturing methods for 2 *MW* scroll case [55].

Case	person-hours	
	2 [ <i>MW</i> ]	250 [ <i>kW</i> ]
Clean Tool	0.660	0.309
Apply Release Agent	0.306	0.1586
Gel Coat	0.306	0.1586
Cut Plies	3.436	1.204
Lay Up Fabric	93.48	26.48
Demold	1.874	1.520
Finishing	1.949	0.616
<b>Totals</b>	<b>100</b>	<b>30.5</b>

Table 4: Process model and person-hours for hand layup and vacuum infusion manufacturing methods for 250 *kW* and 2 *MW* scroll case by HLU.

Component	Method	Materials	Labor	Tooling	Total
Runner	SMC	\$1,808.91	\$229.53	\$248,718.55	\$26,910.29
Guide Vanes	HLU	\$926.08	\$462.54	\$60,290.05	\$7,417.66
	VI	\$945.45	\$251.39		\$7,225.88
Draft Tube	HLU	\$2,660.56	\$2,650.01	\$70,676.69	\$12,378
Penstock	Fil. Winding	\$180.33/ <i>m</i>	\$278.87/ <i>m</i>	\$12,968.91/ <i>m</i>	\$459.20
Scroll Case	HLU	\$11,102.23	\$17,541.63	\$140,250.00	\$43,210.93
	VI	\$11,382.30	\$2,732.37		\$28,070.68

Table 5: Tabulated costs for material, labor and tooling for the 2 *MW* turbine with totals for a 10 part run.

Component	Method	Materials	Labor	Tooling	Total
Runner	SMC	\$1,124.88	\$43.66	\$125,476.48	\$13,716.19
Guide Vanes	HLU	\$1,183.09	\$283.46	\$44,384.98	\$5,905.06
	VI	\$1,197.03	\$204.57		\$5,840.10
Draft Tube	HLU	\$1,130.70	\$1,187.67	\$30,052.93	\$5,323.67
Penstock	Fil. Winding	\$180.33/ <i>m</i>	\$278.87/ <i>m</i>	\$12,968.91/ <i>m</i>	\$459.20
	Spray Up	\$710.39	\$304.45	\$8,849.83	\$1,137.81
Fish Ladder	Pultrusion	\$48.51	\$174.09	\$125,000	\$4,215.18
	<b>Ladder Total</b>	\$758.90	\$478.85	\$133,849.83	\$5,352.99

Table 6: Tabulated costs for material, labor and tooling for the 250 *kW* turbine with totals for single unit in a 10 part run.

